Miner Petrol (2017) 111:569–592
DOI 10.1007/s00710-017-0511-5

ORIGINAL PAPER

Mineralogy and crystallization history of a highly differentiated REE-enriched hypabyssal rhyolite: Round Top laccolith, Trans-Pecos, Texas

L. Christine O'Neill[1] · **Brent A. Elliott**[2] · **J. Richard Kyle**[1,2]

Received: 12 August 2016 / Accepted: 22 March 2017 / Published online: 5 April 2017

Abstract The Round Top hypabyssal rhyolite laccolith is a highly evolved magmatic system, enriched in incompatible elements including REE [Rare Earth Element(s)], U, Be, and F. The Round Top intrusion is part of a series of Paleogene intrusions emplaced as the Sierra Blanca Complex. These intrusions are situated within long-lived, complex tectonic regimes that have been subjected to regional compression and subduction, punctuated by extensional bimodal volcanism. The enrichment in the rhyolite that comprises Round Top is the result of the prolonged removal of compatible elements from the source magma chamber through the emplacement of earlier magmatic events. With the emplacement of each sequential laccolith, the F-rich source magma became more enriched in incompatible elements, with increasing HREE [Heavy Rare Earth Elements(s)] concentrations. The emplacement of Round Top as a laccolith (versus that of an extrusive rhyolitic flow) facilitated the retention of the volatile-rich vapor phase within the magma, forming ubiquitous REE-bearing minerals, mainly yttrofluorite and yttrocerite. The high temperature mineral-vapor phase alteration of the feldspar groundmass was essential to the formation of REE minerals, where the pervasive open pore space was occupied by the late-crystallizing minerals. These late-forming REE-bearing minerals also occur as crystals associated with other accessory and trace phases, as inclusions within other phases, along grain boundaries, and along fractures and within voids. The rhyolite at Round Top and other laccolith intrusions in the Sierra Blanca Complex represent a new sub-type of magmatic rare earth element hosting system.

Keywords Round top · Mineralogy · Rhyolite · Rare earth elements

Editorial handling: D. Harlov

✉ Brent A. Elliott
Brent.elliott@beg.utexas.edu

[1] Department of Geological Sciences, University of Texas, Austin, TX 78712, USA

[2] Bureau of Economic Geology, University of Texas, University Station, Box X, Austin, TX 78713-8924, USA

Introduction

The Trans-Pecos Magmatic Province of Texas hosts more than 100 laccoliths and laccolithic complexes (Henry and McDowell 1986; Corry 1988). The Round Top laccolith is one of several hypabyssal intrusions in the Sierra Blanca Complex (SBC). Although geochemically similar to other peraluminous rhyolite rocks in the SBC, Round Top has generated significant interest due to elevated concentrations in rare earth elements and yttrium (Y + REE), Be, U, and F (Rubin et al. 1987; Price et al. 1990).

Few REE enrichments have been described in association with peraluminous, subalkaline, rhyolitic laccoliths. Round Top presents a unique opportunity to describe the mineralogy and investigate the petrogenesis of a new type of Y + REE mineralization, including the associated enrichment of F, U/Th, and Be (Rubin et al. 1990). REE deposits are presently known to be associated with peralkaline igneous suites, carbonatite, pegmatite, placer(s), iron-oxide Cu-Au, and metamorphosed geologic settings (skarn to high grade), and encompass a wide array of mineralogical forms and concentrations (Long et al. 2010). The occurrence of elevated REE concentrations in peraluminous, subalkaline rhyolites in west Texas entertain the possibility of a new type of REE province.

Geologic setting

Generalities

The SBC is located within the Trans-Pecos Magmatic Province of west Texas (Fig. 1). The province has no definite border, but is approximately bounded by southern New Mexico to the north, the Pecos River to the east, and the Mexico-United States border to the west (Henry and McDowell 1986; Barker 1987; Price et al. 1987, 1990). The southern portion extends south into northern Mexico for an unknown extent (McAnulty 1980; Barker 1977).

Volcanism within the region is bimodal, encompassing both mafic to highly evolved silicic magmatism (Barker 1977; Henry and McDowell 1986; Price et al. 1990; Rubin et al. 1993). Igneous bodies range from voluminous caldera-sourced pyroclastics to intrusive sills and dikes, small volume cones and ring dikes, and shallowly emplaced laccoliths (Barker 1979; Price et al. 1987, 1990). The region is roughly divided into two distinct geochemical sections, a predominantly alkali-calcic volcanic suite to the west (the region in which the SBC is located), and alkalic volcanism to the east (Fig. 1; Henry and Price 1984; Barker 1987; Price et al. 1987).

Magmatic activity in the region was generated in a continental arc environment associated with the subduction of the Farallon Plate beneath the North American Plate. The arc accretion produced bimodal volcanism, extending easterly from the western coast subduction zone (Price et al. 1990; Henry et al. 1991). Trans-Pecos magmatism occurred between 48 and 17 Ma and is mainly divided into two phases, termed early and late (Henry and McDowell 1986; Price et al. 1990; Henry et al. 1989; Rubin et al. 1993). The early phase (48–38 Ma) is characterized by numerous small, silicic-to-mafic igneous intrusions, mafic lava flows, and two minor caldera eruptions (Henry and McDowell 1986; Price et al. 1990). The late phase (38–32 Ma) spanned both the alkalic-calcic and alkalic regions, and comprise the most voluminous episode of Trans-Pecos magmatism (Henry and Price 1984; Henry and McDowell 1986; Price et al. 1990). Volcanism during this period is characterized by numerous silicic-to-mafic intrusions, and large-volume caldera eruptions and associated ash-tuff flows (Henry and Price 1984; Henry and McDowell

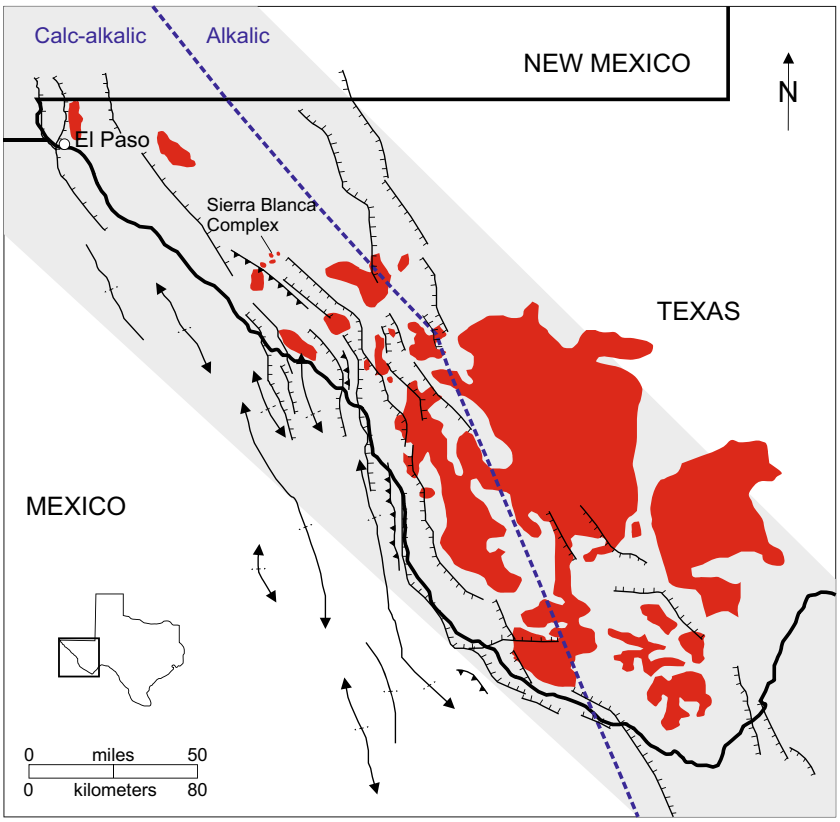

Fig. 1 Location map of the Sierra Blanca Complex (SBC) relative to major geologic structures within the Trans-Pecos Magmatic Province. The Trans-Pecos Magmatic Province (*red*) is bounded to the north by New Mexico, to the east by the Pecos River, to the west by the Texas-Mexico border, and continues south into Mexico. The region is divided into two geochemical affinities (*dashed blue line*): calc-alkaline volcanic suites to the west (the region where the SBC is located), and alkaline volcanism to the east. The Texas Lineament Zone spans across the Trans-Pecos region, representing a broad ~80-km wide zone of parallel trans-tensional faulting (*gray shaded region*). Map modified from Muehlberger (1980) and Price et al. (1990)

1986; Price et al. 1990). Basin and Range extension was initiated by a change in regional stress around 31 Ma. Subsequent normal faulting in the region began at approximately 24 Ma (Price et al. 1990). Small volume mafic volcanism accompanied the early stages of rifting, with the youngest episode dated at 17 Ma (Price et al. 1990).

Prior to Trans-Pecos magmatic activity, the region underwent Laramide deformation, including predominately north-northwest folding and thrusting (Wilson 1980; Price et al. 1990). This tectonic activity is responsible for the gentle dip (~15° SW) of the Cretaceous units, into which the SBC was emplaced (Price et al. 1990). Transecting the Trans-Pecos Magmatic Province is the Texas Lineament Zone; a regional series of large-scale parallel geologic features, spanning a 80-km wide zone within the western portion of Texas and continuing into Mexico. The zone represents long-term and ongoing periodic tectonic activity, dominated by dip-slip fault movement, beginning approximately at 1.4 Ga, and continuing through to the present (Muehlberger 1980). The Sierra Blanca and Van Horn area is the type locality for this regional Texas Lineament Zone trend as defined by Albritton and Smith (1965). Muehlberger (1980) positioned the SBC along the proposed northern boundary of the Texas Lineament Zone, within the downthrown portion of a tectonic block. The downthrown block is bounded by the regionally north- trending normal Rim Rock Fault to the north and an unnamed, more minor normal fault to the south. Contrary to this, Albritton and Smith (1965) and Price et al. (1990) placed the SBC along the eastern footwall side of a large regional scale thrust fault (Fig. 1). The Trans-Pecos region has undergone a complex tectonic history, which most likely includes the reactivation of numerous faults during different tectonic episodes, thus obscuring the exact nature of fault movement in the area. These tectonic episodes have contributed to the formation and location of many of the igneous features within the province, including the SBC. The SBC area has been the site of regional scale thrusting and orogenic activity during the Proterozoic, high-angle normal faulting during the Late Paleozoic, folding and thrusting during the Laramide orogeny, and on-going Basin and Range extension. Sierra Blanca Peak, and presumably the rest of the Sierra Blanca laccoliths were emplaced during the main phase of Paleogene bimodal Trans-Pecos magmatic activity at 36.2 ± 0.6 Ma (K/Ar in biotite; Henry and McDowell 1986).

Sierra Blanca complex (SBC)

The SBC is a series of five peraluminous rhyolite and rhyolite porphyry laccoliths emplaced in an arcuate pattern. All of the laccoliths are aphanitic to slightly porphyritic, thus the common use of rhyolite (cf. microgranite) for their general description. The laccoliths extend over an area of approximately 90 km^2 southwest of the Finley Mountains and north of the Quitman Mountains (Fig. 2; Henry and McDowell 1986). The largest laccolith, Sierra Blanca, was emplaced at 36.2 ± 0.6 Ma (Henry and McDowell 1986; Matthews and Adams 1986). Emplacement ages of the four other laccoliths have not been determined, but a relative emplacement sequence can be interpreted through major- and trace-element differentiation patterns. Based on the increasing enrichment of REE, especially the increasing ratio of HREE to LREE [Light Rare Earth Elements(s)] among the five laccoliths, Triple Hill was emplaced first, followed sequentially by Sierra Blanca, and then Round Top, Little Sierra Blanca, and Little Round Top contemporaneously (Shannon 1986; Shannon and Goodell 1986; Price et al. 1990). The small differences in highly evolved compositions and rapid cooling textures suggest the timing between emplacement and duration of emplacement was relatively short.

Round Top laccolith

Round Top is the most westerly of the five laccoliths and covers an area of approximately 2.4 km^2 (Fig. 2). The laccolith has an elevation of 1747 m with an approximate maximum thickness of 396 m. The laccolith is composed of four variations of peraluminous, subalkaline rhyolite that differs slightly by color, mineralogy, and texture (including mottled forms). Compositionally, the rhyolite is very homogenous (see Table 1), with an average wt% SiO_2 73.67, A/CNK [molar $Al_2O_3/(CaO + Na_2O + K_2O)$] 1.04 and A/NK [molar $Al_2O_3/(Na_2O + K_2O)$] 1.08, wt% FeO^{tot}/(wt% FeO^{tot} + wt% MgO) ratio 0.96, similar wt% K_2O and Na_2O (4.27 and 4.84, respectively). REE concentrations are elevated (REE + Y = 380 ppm), especially HREE (La/Yb = 0.31; see Fig. 3).

The laccolith has an asymmetrical convex morphology in cross-section, and is circular on the mapped surface with a peaked dome. On the northern flank, the northeast portion has been eroded to expose the underlying diorite sill and limestone host rock. The northeast flank ends abruptly into a sedimentary host rock saddle, across which Little Round Top laccolith is located. The southern flank is steep, and grades into a shallow slope at the base, extending laterally onto the desert floor. The rhyolite is blocky and fragmented, and locally cemented by multiple generations of fluorite, calcite, microcrystalline quartz, and clay.

Sampling and analytical techniques

A total of 373 samples were collected from locations at Round Top, Little Round Top, and Sierra Blanca (O'Neill

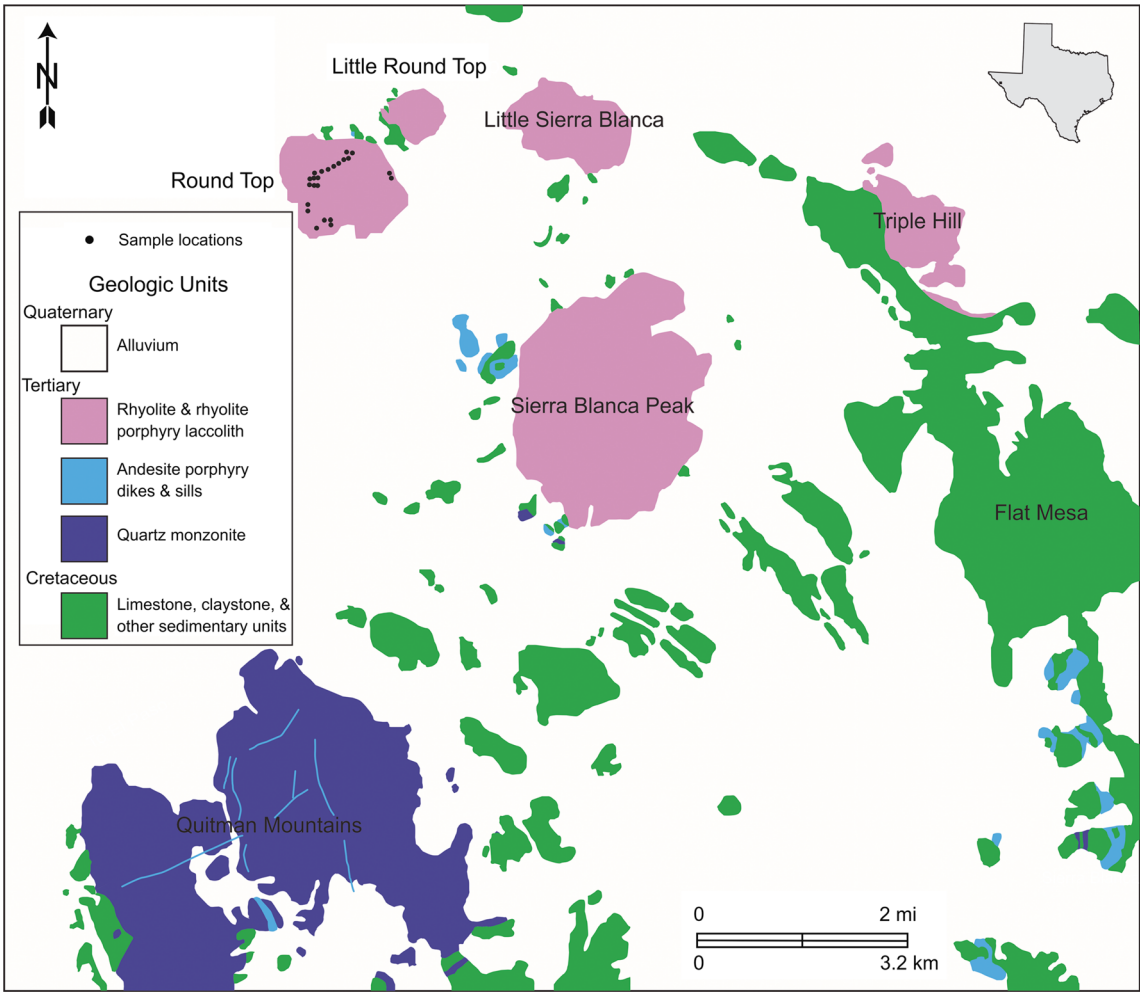

Fig. 2 Geologic map of the Sierra Blanca peaks, modified after McAnulty (1980). The laccolith group consists of Sierra Blanca Peak, Round Top, Little Round Top, Little Sierra Blanca, and Triple Hill

2014). Samples were collected from outcrops, road cuts, and from reverse circulation (RC) cuttings from drilling provided by Texas Rare Earth Resources LLC (a company doing exploratory drilling). Materials sampled included unaltered rhyolite, altered rhyolite, fluorite, calcite, and rhyolite breccia cemented with fluorite, calcite, and microcrystalline quartz. RC samples were collected from representative intervals from nine drill holes that form two perpendicular cross sections across the laccolith (Fig. 2). The cross sections form approximately northwest and northeast linear transects and represent a total of 1554 m of drilling.

Whole-rock geochemical major and trace element analyses were conducted by a lithium borate fusion and dilute acid digestion of 0.2 g sample pulp followed by inductively coupled plasma mass spectroscopy (ICP-MS). Total carbon and sulfur were analyzed by loss of ignition (LOI) by sintering at 1000 °C and Leco analysis.

Petrographic work was conducted using Zeiss Axioskop 40 transmitting light petrographic microscopes utilizing Sony Handycam E-mount NEX-VG10 cameras. 43 petrographic thin sections attached to a glass slide were produced for use in this study from samples collected during fieldwork. 18 thin sections were partially stained with sodium cobaltinitrite to discern the K-rich portions of the sections.

Scanning electron imaging was conducted using a JEOL JSM-6490LV scanning electron microscope (SEM), and a Phillips/FEI XL30 environmental SEM (ESEM). The SEM work included use of back-scattered electrons (BSE) detectors for sample imaging, in conjunction with an standardless energy dispersive X-ray spectroscopy (EDS) detector for qualitative and quantitative elemental analysis of samples using AztecEnergy EDS Software. Quantitative EDS measurements were taken with an acceleration voltage of 15 or 20 kV, and a spot size less than 5, 2 or 1 μm, depending on the grain size. The ESEM analyses utilized cathodoluminescence (CL), BSE, and SEM detectors to image elemental and compositional incongruities within samples.

Table 1 Average whole-rock major-element and trace-element geochemistry (ICP-MS) of the Round Top rhyolite

Major-element data			Trace-element data					
Constituent	Content (wt%)	2 σ	Element	Content (ppm)	Element	Content (ppm)	Element	Content (ppm)
SiO_2	73.67	0.42	Li	0	Nb	360	Th	169
TiO_2	0.02	0.00	Be	28	Mo	1	U	38
Al_2O_3	13.59	0.25	Sc	1	Ag	0	La	16
Fe_2O_3	1.54	0.39	V	11	Cd	0	Ce	57
FeO	0.54	0.10	Cr	2	Sn	142	Pr	8
MnO	0.06	0.01	Ni	1	Sb	1	Nd	21
MgO	0.09	0.08	Co	0	Cs	50	Sm	7
CaO	0.25	0.16	Cu	1	Ba	49	Eu	0
Na_2O	4.84	0.10	Zn	475	Hf	79	Gd	7
K_2O	4.27	0.20	Ga	69	Ta	59	Tb	2
P_2O_5	0.02	0.00	As	6	W	4	Dy	22
F	0.39	0.20	Se	1	Au	0	Ho	6
Total	99.27		Rb	1850	Hg	0	Er	25
			Sr	63	Tl	2	Tm	6
A/CNK	1.04		Y	150	Pb	112	Yb	47
A/NK	1.08		Zr	1038	Bi	2	Lu	7

All values are averages of 37 single analyses

A/CNK = molar [Al_2O_3/(CaO + Na_2O + K_2O)]

A/NK = molar [Al_2O_3/(Na_2O + K_2O)]

Results

Accessory phases comprise 7–9% of the rhyolite, and include Fe-rich biotite, magnetite, hematite, and zircon. The Fe-rich biotite, zircon, and hematite are too small to be discernable without a microscope. The magnetite is typically larger than the other accessory phases and is therefore visible with the aid of a hand-lens, but is more easily observed with the aid of a petrographic microscope.

Feldspar

Plagioclase feldspar phenocrysts comprise 8–14% of the rhyolite and occur as subhedral to euhedral albite rectangular

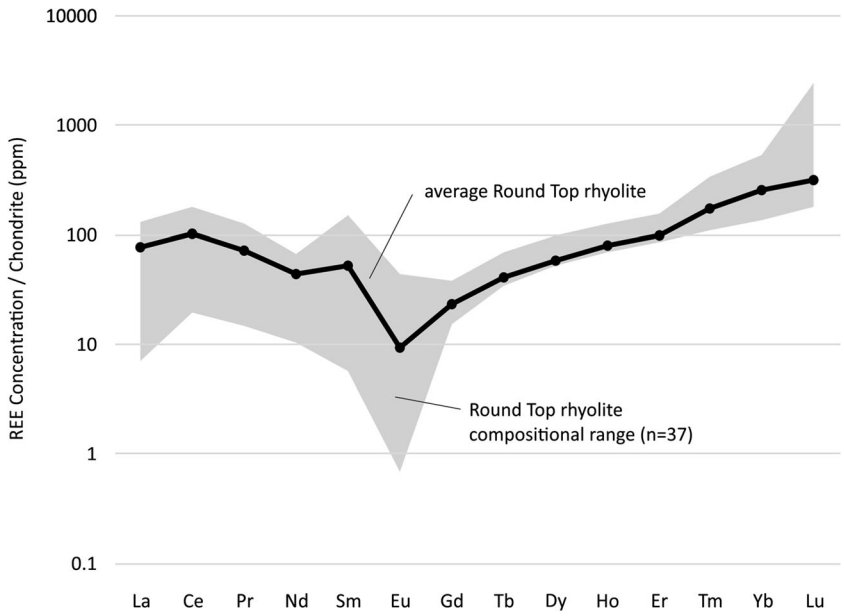

Fig. 3 Average REE composition (*black line*), compared with the range of Round Top rhyolite compositions (*grey shaded area*), normalized against chondrite (Boynton 1984)

lathes with potassic feldspar overgrowths. These lathes with overgrowths occur in clusters, as penetrating twins, or as individual phenocrysts (Fig. 4). The potassic mantles can have an additional albitic overgrowth, although this is rare. The outer portion of the albite, before the K-feldspar overgrowth, is equant and without reaction textures, indicating a lack of albite dissolution before the formation of the potassic feldspar overgrowth. The plagioclase phenocrysts range from 20 to 120 μm in length. In crossed polarized light, the plagioclase commonly displays an array of albitic and/or Carlsbad twinning. CL imaging and EDS analysis indicate relatively homogenous compositions with little variation, and no Ca-rich feldspar was observed. The feldspar lathes are typically the largest of the phenocrysts, when both cores and overgrowths are considered. The morphology of the inner core is euhedral with no observable corrosion or embayment along the core-mantle transition. Plagioclase compositions are sodic with compositions ranging from pure albite (Ab_{100}) to Ab_{95} (see Table 2).

K-feldspar phenocrysts constitute 48–52% of the rhyolite, and is found in two forms, 1) as a rind mantling a more sodic plagioclase core (60%), and 2) as euhedral to subhedral phenocrysts with distinct hourglass sector zonation (40%; Fig. 5). The clarity of the K-feldspar phenocrysts and overgrowths in plane polarized light and crossed polarized light is typically diminished due to a pervasive turbidity, causing the phenocrysts to appear near-opaque.

The mantling population of K-feldspar ranges from 10 to 60 μm at the widest point. Generally, the smaller the inner sodic core, the wider the outer potassic rim. CL imaging and EDS analyses suggest portions of the overgrowth are more sodic-rich versus potassic. In CL, these sodic portions appear as dark gray "stringers" in normal CL gray-scale, and typically match the shade of the inner plagioclase core. The overgrowths generally display a ragged, corroded appearance on the outer edges, and a smooth continuous contact with the interior plagioclase feldspar (Fig. 6). They are commonly too turbid in appearance to distinguish any form of extinction under cross polars.

The hourglass feldspar phenocrysts have lengths ranging from 75 to 200 μm. The hourglass feldspars display internal symmetry and clarity varying from highly discernable and

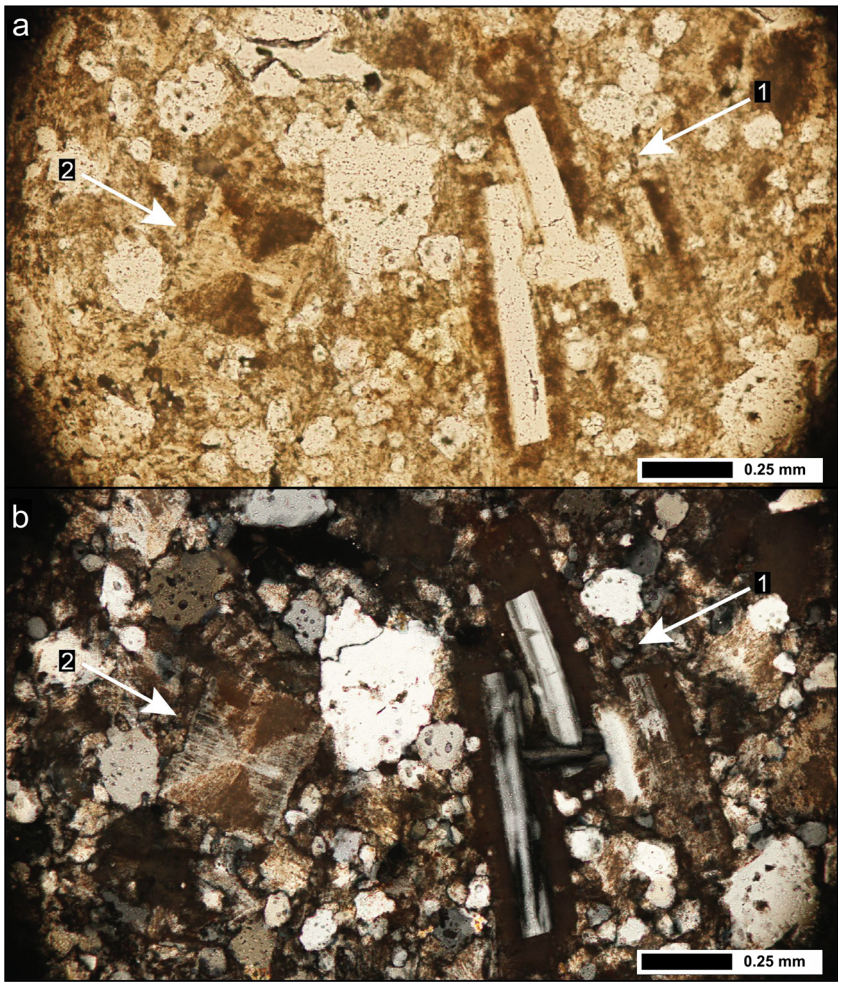

Fig. 4 Photomicrographs examples of typical K-feldspar phenocrysts in (**a**) plane polarized light and (**b**) under cross polars. K-feldspar occurs in two forms: (1) as an overgrowth to a more sodic feldspar cores, and (2) as an hourglass textured phenocryst

Table 2 Quantitative EDS analyses, cation proportions and end member compositions of feldspars from the Round Top rhyolite

Analysis	1	2	3	4	5	6	7	8	9	10
K-feldspar										
Data obtained by EDX analysis (all values in wt%):										
SiO_2	75.4	69.9	67.3	82.6	69.3	69.5	70.2	70.1	69.2	69.7
Al_2O_3	15.4	17.6	19.2	10.7	18.1	17.9	17.4	17.6	18.2	17.9
CaO	0.00	0.00	0.00	0.00	0.00	0.00	0.00	0.00	0.00	0.00
Na_2O	4.34	1.60	2.41	3.36	1.44	1.01	1.66	1.55	4.00	2.55
K_2O	4.82	10.9	11.1	3.32	11.2	11.6	10.8	10.8	8.57	9.81
Total	100.0	100.0	100.0	100.0	100.0	100.0	100.0	100.0	100.0	100.0
Mineral formulae calculated on the basis of 8 oxygens (all values in a.p.f.u.):										
Si	3.25	3.12	3.02	3.49	3.09	3.10	3.13	3.12	3.08	3.10
Al	0.78	0.92	1.02	0.53	0.95	0.94	0.91	0.92	0.95	0.94
Ca	0.00	0.00	0.00	0.00	0.00	0.00	0.00	0.00	0.00	0.00
Na	0.36	0.14	0.21	0.28	0.13	0.09	0.14	0.13	0.34	0.22
K	0.27	0.62	0.64	0.18	0.64	0.66	0.61	0.61	0.49	0.56
Total	4.67	4.80	4.89	4.47	4.81	4.80	4.79	4.79	4.86	4.82
Calculated end-member compositions (all values in mol%):										
An	0.00	0.00	0.00	0.00	0.00	0.00	0.00	0.00	0.00	0.00
Ab	57.78	18.15	24.81	60.66	16.41	11.73	18.97	17.91	41.49	28.33
Or	42.22	81.85	75.19	39.34	83.59	88.27	81.03	82.09	58.51	71.67
Plagioclase										
Data obtained by EDX analysis (all values in wt%):										
SiO_2	70.8	70.9	71.9	71.5	70.1	68.6	70.7	70.3	70.0	68.5
Al_2O_3	18.7	19.1	18.2	18.6	18.8	19.6	19.4	19.2	18.3	19.4
CaO	0.00	0.00	0.00	0.00	0.00	0.00	0.00	0.00	0.00	0.30
Na_2O	10.4	10.0	9.97	9.90	10.5	11.0	9.96	10.4	10.8	11.0
K_2O	0.00	0.00	0.00	0.00	0.61	0.70	0.00	0.00	0.91	0.70
Total	100.00	100.00	100.00	100.00	100.00	100.00	100.00	100.00	100.00	100.00
Mineral formulae calculated on the basis of 8 oxygens (all values in a.p.f.u.):										
Si	3.06	3.06	3.10	3.08	3.05	3.00	3.05	3.05	3.05	3.00
Al	0.96	0.97	0.92	0.95	0.96	1.01	0.99	0.98	0.94	1.00
Ca	0.00	0.00	0.00	0.00	0.00	0.00	0.00	0.00	0.00	0.01
Na	0.87	0.84	0.83	0.83	0.88	0.93	0.83	0.88	0.91	0.94
K	0.00	0.00	0.00	0.00	0.03	0.04	0.00	0.00	0.05	0.04
Total	4.89	4.87	4.86	4.86	4.93	4.98	4.87	4.90	4.96	4.99
Calculated end-member compositions (all values in mol%):										
An	0.00	0.00	0.00	0.00	0.00	0.00	0.00	0.00	0.00	1.40
Ab	100.00	100.00	100.00	100.00	96.30	96.01	100.00	100.00	94.74	94.62
Or	0.00	0.00	0.00	0.00	3.70	3.99	0.00	0.00	5.26	3.98

a.p.f.u. atoms per formula unit

well defined to poorly defined and irregular. This feldspar hourglass texture was first described to be an attribute of the Round Top rhyolite by Barker (1980). Under cross polars, discrete grains typically display a double undulatory extinction, sweeping inward through one opposing set of hourglass structures, then passing outward through the opposite pair, with continued rotation of the stage. EDS analyses confirmed that the hourglass type phenocrysts are predominately composed of K-feldspar, although one of the two hourglass sectors typically contains relatively more Na. With CL, the two hourglass sections are visually evident as differing shades of gray caused by the slight compositional difference forming the sector zonation. Compositionally, the sectors are too similar to be distinguished with BSE or SE imaging. K-feldspar compositions range from $Or_{88}Ab_{12}$ to $Or_{39}Ab_{61}$ (see Table 2).

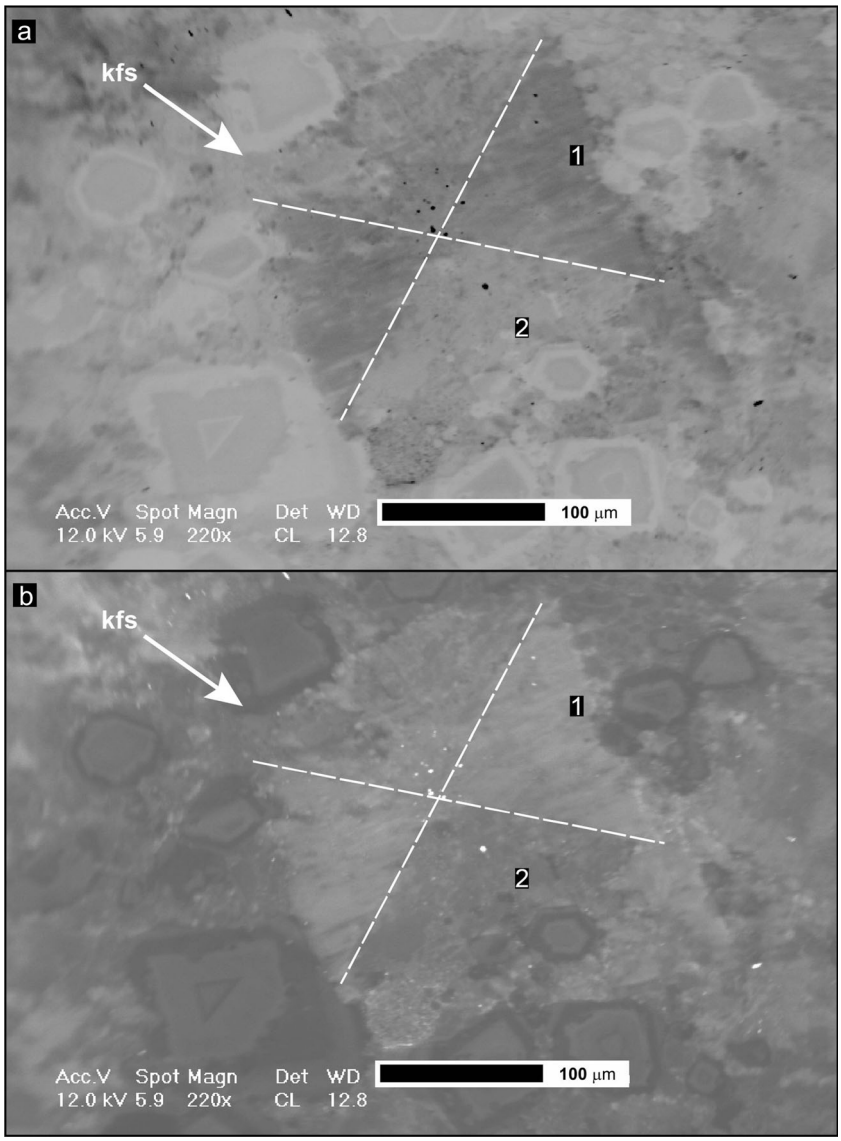

Fig. 5 CL image of the hourglass type K-feldspar (kfs) phenocryst with distinct sector zonation. The *white dashed lines* denote the approximate boundaries between the two internal hourglass structures. In normal CL (**a**), the K-rich portion (1) appears as a *darker gray*, whereas the K plus Na portion (2) appears as a *lighter gray*

Quartz

Quartz phenocrysts comprise 28–30% of the rhyolite and occurs as colorless anhedral to subhedral phenocrysts that typically range from 20 to 150 µm in diameter (Fig. 7). The core is equant, euhedral to subhedral, high temperature beta quartz. Beta quartz, the higher temperature quartz polymorph, forms at a minimum temperature of 573 °C at 1 atm (Nesse 2000). The Round Top rhyolite probably formed at typical rhyolite temperatures, well above this minimum melt temperature. Due to subsequent decreased pressure and temperature conditions, the quartz phenocrysts have been pseudomorphed to the trigonal, lower temperature form of alpha quartz (Fig. 7).

Most of the quartz phenocrysts exhibit a pseudoconcentric ring of melt inclusions of a purplish hue (in plane polarized light), first documented by Barker (1980; Fig. 8). These are more easily discernible with the CL detector. Compositionally, these melt inclusions are K-, Na-, Al- and Si-rich, similar to the groundmass.

CL analyses show that following, and intermingled with, the inclusion ring is an overgrowth of late-stage anhedral magmatic quartz (Fig. 7). The quartz overgrowth typically is highly embayed and undulatory along the outer edge, due to subsequent corrosive processes. The differences between the inner and outer portions of the quartz phenocrysts, when viewed with CL, suggest slight compositional and/or structural variations, which are not detectable with the EDS. Further analyses with the CL detector on the ESEM determined that the inner core is typically oscillatory zoned and appears as a darker gray to the outer portion when viewed in normal CL mode (Fig. 9). The late-stage overgrowth of quartz varies greatly in thickness, and may range from 10 to 60 µm for phenocrysts of similar size. One phenocryst of quartz with rutile inclusions was observed as an inclusion within a feldspar glomerocryst.

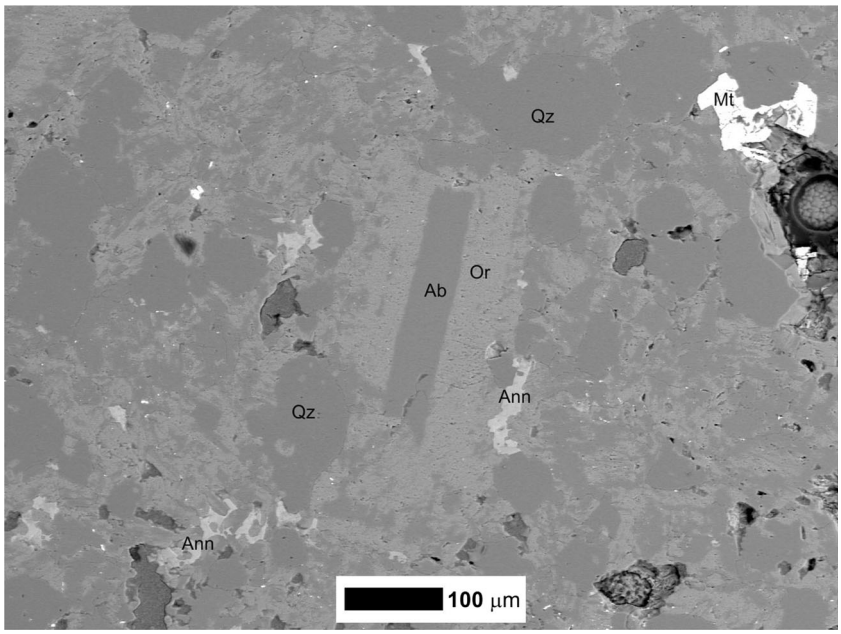

Fig. 6 BSE image of K-feldspar (Or) as an overgrowth to a plagioclase feldspar (Ab) core. Note the angular nature of the exterior edges of the K-feldspar overgrowth, indicating late corrosion due to disequilibrium. Additionally, the transition from the plagioclase core to the potassic overgrowth is abrupt with a sharp mineral contact. Under cross polars, the Carlsbad twinning of the plagioclase is apparent

Lastly, the abundance of subhedral to anhedral quartz that comprises the groundmass is more readily apparent when viewed with the CL detector.

Biotite

Fluorine-rich Fe-rich biotite (annite; 10–100 μm) is the least abundant of the major phases, comprising 4–5% of the rhyolite. The Fe-rich biotite typically occurs as subhedral to anhedral phenocrysts interstitial to the groundmass or adjacent to other more euhedral phenocrysts. In plane polarized light, the annite displays a range of moderate pleochroism, alternating from a pale yellow-green to a dark brown-green. The outer edges of the phenocrysts are typically ragged, irregular, embayed, and undulatory, conforming to the shape of adjacent, earlier formed phenocrysts. Mineral chemical analyses show Fe/(Fe + Mg) ratios of 100, 1.05–3.52% oxide Na_2O, 3.06–7.39% oxide K_2O, and very high F contents, ranging from 1.57–6.13% (see Table 3).

This morphology suggests late crystallization in the petrogenetic sequence, potentially contemporaneous with the groundmass. In some instances, the annite displays graphic-texture edges, indicating rapid nucleation during undercooling. Inclusions of quartz, magnetite, hematite, and yttrofluorite have been identified with EDS analyses within the Fe-rich biotite. The biotite commonly displays compositional zonation within a single crystal, visible as a darker gray color within the interior portion of the grain mantled by lighter gray under BSE imaging. Compositional zonation is too subtle to be detected by EDS. Price et al. (1990) described the presence of two micas within the Sierra Blanca rhyolite, an Fe-Mg biotite and a Li-rich Fe-rich biotite. The presence of only fluorine-rich Fe-rich biotite at Round Top correlates well with the more evolved whole-rock composition when compared to Sierra Blanca.

Magnetite and hematite

Magnetite and hematite comprise approximately 2–3% of the rhyolite. Magnetite and hematite commonly occur in conjunction with one another, where hematite is often a direct product of magnetite oxidation. There appears to be a trend in magnetite-hematite content, where the amount of hematite increases at the expense of magnetite from gray to purple to red to tan rhyolite variations. This effect is visually apparent by the increasing turbidity of the rhyolite when viewed with a transmitting light microscope (Fig. 10). Additionally, the integrity of the magnetite phenocrysts decreases between the rhyolite variations, presumably due to the incomplete oxidization of the magnetite during the formation of hematite. Magnetite that is partially oxidized exhibits pitting and embayments that are typically filled with, or surrounded by, a halo of hematite (Fig. 10). This partial oxidation of the magnetite increases in abundance from the gray to red rhyolite variations. There were no magnetite-hematite phenocrysts observed in the tan rhyolite, although small inclusions of magnetite are moderately abundant within the groundmass and hematite is present within the groundmass and pore spaces.

Magnetite occurs as euhedral to subhedral phenocrysts that range from 10 to 150 μm and as microcrysts within the groundmass. Magnetite commonly occurs as anhedral inclusions in other phenocrysts ranging from 1 to 5 μm in size. Approximately 70% of the magnetite occurs in close

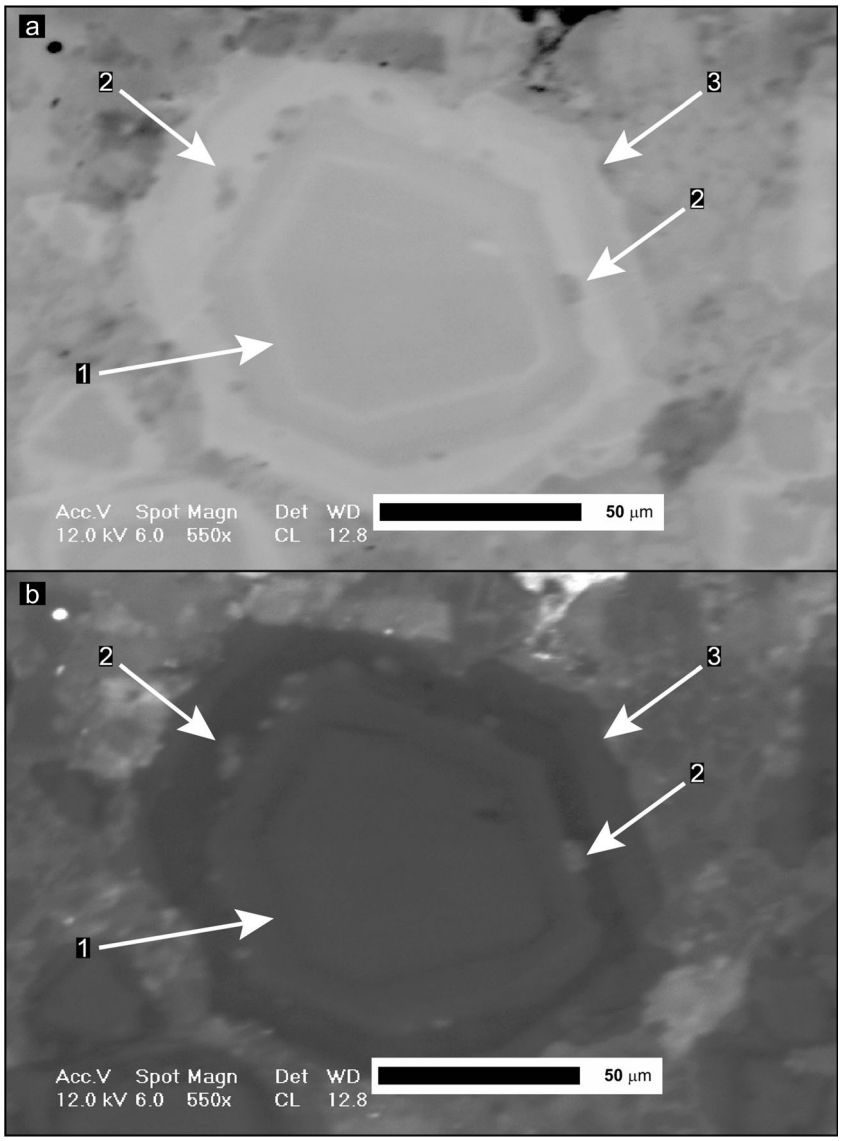

Fig. 7 CL image of a typical three-part quartz phenocryst comprised of an inner zoned hexagonal quartz core (1), followed by a concentric ring of melt inclusions (2), overgrown by a later stage subhedral to anhedral quartz (3)

association with other accessory phases, including hematite, zircon, tantalite, columbite, cassiterite, changbaite, and Y ± REE fluorides. The trace phases that occur in conjunction with the magnetite are typically entrained as inclusions and/or just adjacent to the phenocryst, and is often reflected in microprobe analyses (Fig. 11; see Table 4). Titanium abundances in iron oxide compositions are relatively low, ranging from 0 to 1.25%. Under reflected light, magnetite is typically associated with a distinct red hematitic halo.

Hematite is visible in hand sample as red spots throughout the purple and red rhyolite. Hematite occurs in two forms, 1) as halos around magnetite phenocrysts, and 2) as inclusions within K-feldspar groundmass. The hematite halos are up to 100 μm and consist of micro-crystals ranging from <1–2 μm in diameter. The hematite halos are distinctly noticeable in purple rhyolite, visible as red spots in hand sample. Hematite inclusions are least abundant within the gray rhyolite and increase in the purple and red varieties. In transmitted light, the hematite appears as red micro-inclusions scattered throughout the groundmass. Within all of the rhyolite types when viewed in plane polarized light, the hematite is a red-brown color and distinctly red in reflected light. The hematite inclusions occur most commonly near or in association with other accessory and trace phases, such as magnetite, Fe-rich biotite, zircon, and thorite (Figs. 11 and 12).

Zircon

Zircon comprises ≤0.5% of the rhyolite, based on petrography and geochemical analyses (O'Neill 2014). Within the Round Top rhyolite, two zircon populations exist, 1) thorite inclusion-rich and 2) thorite inclusion-poor populations (Fig. 12, see Table 5). The thorite inclusion-rich population appears to be the more abundant. Both populations range from

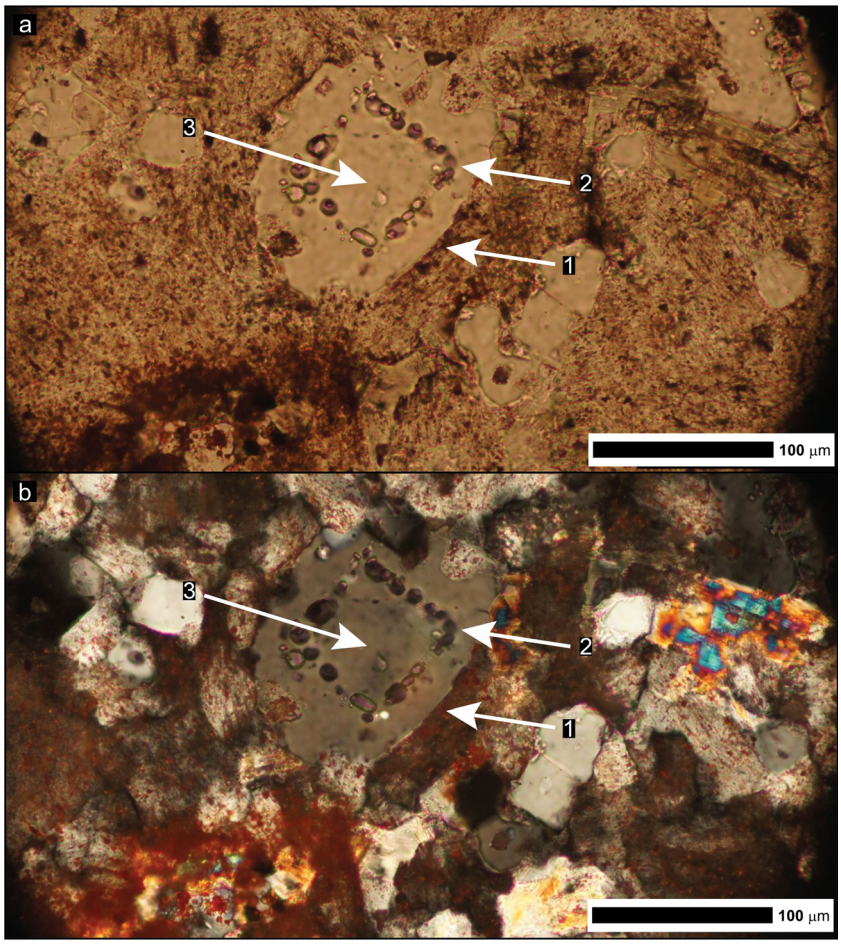

Fig. 8 Photomicrographs of a quartz phenocryst with concentric melt inclusion ring under (**a**) plane polarized light and (**b**) cross polars. Quartz phenocrysts are typically comprised of an outer quartz overgrowth (1), followed by a concentric ring of melt inclusions (2) enriched in Na, K, Al, and Si, and a quartz core (3). The inclusions appear *purple* under plane polarized light and under cross polars, and are typically round to oblong in shape. The inclusions appear to be melt inclusions where no obvious vapor phase or daughter crystals have been observed

10 to 40 μm in length and are enriched in Hf, U, and Th. Most grains are anhedral, although a few instances of subhedral to euhedral phenocrysts have been observed (Fig. 13). These well-formed phenocrysts are rare, but when they do occur they are typically highly embayed with corroded irregular outer edges. Individual subhedral to anhedral crystals are typically amorphous and have stinger-like apophyses (first noted by Rubin et al. 1989a, b). The subhedral to anhedral zircons are late-stage, and typically occur in clusters with each other and other accessory and trace phases, such as magnetite, hematite, tantalite, and yttrocerite (Fig. 11). Many of the zircon phenocrysts contain abundant void spaces where inclusions were plucked during thin section preparation. Thorite commonly occurs adjacent to zircon (Fig. 13), and inclusions (where present) may comprise up to 20% of the zircon phenocryst.

Rubin et al. (1989a, b) presented the hypothesis that the two populations of zircon represent an initial magmatic population (thorite inclusion-rich), and a later population introduced by migrating hydrothermal fluids (thorite inclusion-poor). Rubin et al. (1989a, b) noted the common presence of late-stage hydrothermal zircons within the fluorite replacement in the underlying limestone, but not within the Round Top rhyolites. Both populations (the thorite inclusion-rich and inclusion-poor) were observed in the Round Top rhyolites, commonly in close proximity to one another.

Groundmass mineralogy

The rhyolite groundmass, <10% of the total rock volume, is composed of (in decreasing order), subhedral to anhedral K-feldspar, plagioclase feldspar, and quartz. Staining reveals the pervasive abundance of K within the groundmass of all of the rhyolite types, although the red rhyolite has a notably higher abundance of K-rich mineralogy than the purple and gray varieties. When stained, approximately 20% of the gray rhyolite groundmass appears yellow, 30% for the purple, and 40% for the red.

These percentages are approximate and attempt to omit the K-rich phenocrysts from the estimations. Within the gray rhyolite, the yellow portions of the groundmass appear as isolated pockets, surrounded by areas lacking abundant K. This differs greatly from the red rhyolite, in which the K-rich portions appear ubiquitous throughout the entirety of the groundmass. This is a surprising textural difference as the gray, purple, and red rhyolites all have an overall similar concentration of K_2O (approximately 4 wt%). In addition to emphasizing the K-rich

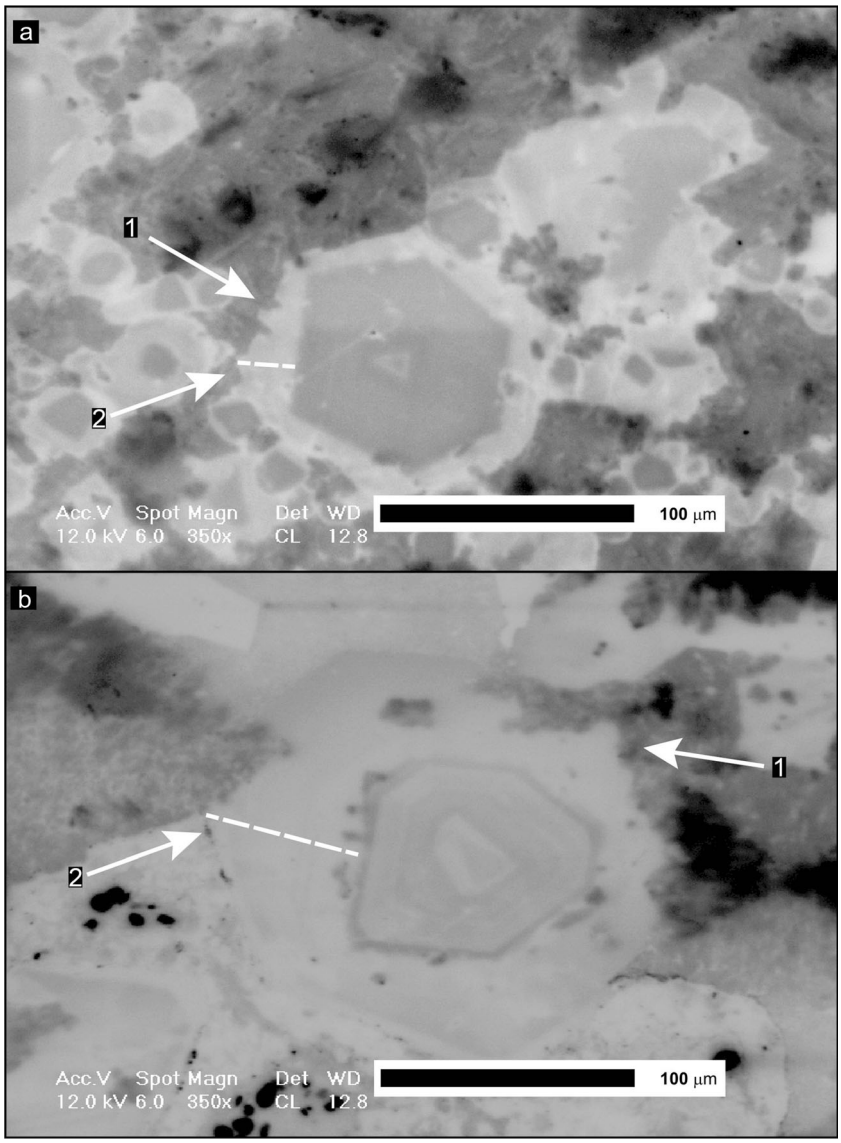

Fig. 9 CL images of the three-part quartz phenocrysts with varying outer overgrowth thickness and zoned interior cores. The thickness of the late stage quartz overgrowth rims vary greatly (2) and have been observed to range from 10 to 60 μm in diameter at the widest point for phenocrysts of approximately the same size. The outer edge of the late-stage overgrowth is typically embayed and undulatory (1), denoting rapid crystallization and/or later corrosion of the rim due to disequilibrium

pockets within the groundmass, staining accentuates the K mantles of the plagioclase feldspar laths and the more K-rich quadrants of the hourglass feldspars.

The groundmass of the rhyolite is dominated by intergrown anhedral patches of K and plagioclase feldspar with subhedral to anhedral quartz. The pores within the K and plagioclase feldspars commonly appear in linear patterns, probably along cleavage planes. The relative proportions of K-feldspar to plagioclase and quartz are approximately the same between the gray, purple, and red rhyolite. The tan rhyolite is highly porous compared to the other three and appears to contain considerably less K within the groundmass. The gray, purple, and red rhyolites display a characteristic groundmass intermingled feldspar texture. Although compositionally very similar, there appears to be slight textural differences between the groundmass of the different rhyolites. The gray and tan rhyolites have slightly more quartz within the groundmass (25%) than the purple and red (15–20%). Additionally, the groundmass of the purple rhyolite appears to contain a slightly less intermingled feldspar texture, whereas the red rhyolite appears to contain the largest amount of the intermingled feldspar texture. Within all types of the rhyolite, the groundmass contains inclusions of accessory and trace phases, particularly within the K-feldspar.

Trace minerals

Y-Ce-REE-F phases

Yttrofluorite [(Ca, Y, HREE)F_2] and yttrocerite [(Ca, Ce, LREE, HREE)F_2] are the two main REE-fluorides identified within the Round Top rhyolites. Price et al. (1990) also identified an unknown Ca-Th-Pb-REE fluoride of limited abundance (X-fluoride). The variation in composition and concentrations of the REE and additional elemental components

Table 3 Quantitative EDS analyses, cation and volatile proportions of biotite from the Round Top rhyolite

Biotite									
Analysis	1	2	3	4	5	6	7	8	9
Data obtained by EDX analysis (all values in wt%):									
SiO_2	53.9	61.1	51.3	53.4	56.3	49.4	67.9	51.5	50.8
TiO_2	0.00	0.00	0.00	0.00	0.00	0.00	0.00	0.77	0.00
Al_2O_3	22.3	15.8	20.9	21.1	19.9	10.3	8.89	17.9	19.9
Fe_2O_3	8.00	9.95	9.56	8.52	5.88	15.3	15.8	12.7	8.05
MgO	0.00	0.00	0.00	0.00	0.00	0.00	0.00	0.00	0.00
CaO	0.00	0.00	0.00	0.00	0.00	0.00	0.00	0.00	0.00
MnO	1.20	1.12	1.76	1.48	1.54	2.35	0.00	1.78	1.69
FeO	0.89	1.11	1.06	0.95	0.65	1.71	1.75	1.41	0.89
Na_2O	1.14	2.60	2.15	1.41	3.52	2.57	1.06	2.81	1.95
K_2O	6.47	5.20	6.06	7.39	5.59	7.23	3.06	7.25	6.57
F	6.13	3.11	5.23	5.75	5.38	2.84	1.57	3.88	8.20
H_2O	0.77	1.57	0.92	0.84	0.95	1.30	2.00	1.26	0.16
Total	100.77	101.57	98.98	100.84	99.73	93.06	102.00	101.26	98.22
F = O	2.58	1.31	2.20	2.42	2.27	1.19	0.66	1.63	3.45
Total	98.19	100.26	96.77	98.42	97.46	91.87	101.33	99.63	94.77
Mineral formulae calculated on the basis of 11 oxygens and 2 OH, F, Cl (all values in a.p.f.u.):									
Si	3.63	3.97	3.56	3.63	3.79	3.75	4.30	3.54	3.63
Al^{IV}	0.37	0.03	0.44	0.37	0.21	0.25	−0.30	0.46	0.37
T-site	4.00	4.00	4.00	4.00	4.00	4.00	4.00	4.00	4.00
Al^{VI}	1.40	1.19	1.26	1.32	1.37	0.67	0.96	0.98	1.30
Ti	0.00	0.00	0.00	0.00	0.00	0.00	0.00	0.04	0.00
Fe^{3+}	0.41	0.49	0.50	0.44	0.30	0.88	0.75	0.66	0.43
Fe^{2+}	0.05	0.06	0.06	0.05	0.04	0.11	0.09	0.08	0.05
Mn	0.07	0.06	0.10	0.08	0.09	0.15	0.00	0.10	0.10
Mg	0.00	0.00	0.00	0.00	0.00	0.00	0.00	0.00	0.00
Y-site	1.93	1.80	1.93	1.89	1.80	1.81	1.81	1.87	1.89
Ca	0.00	0.00	0.00	0.00	0.00	0.00	0.00	0.00	0.00
Na	0.15	0.33	0.29	0.19	0.46	0.38	0.13	0.37	0.27
K	0.56	0.43	0.54	0.64	0.48	0.70	0.25	0.64	0.60
X-site	0.71	0.76	0.82	0.83	0.94	1.08	0.38	1.01	0.87
F	1.31	0.64	1.15	1.24	1.15	0.68	0.31	0.84	1.85
OH	0.69	1.36	0.85	0.76	0.85	1.32	1.69	1.16	0.15

a.p.f.u. atoms per formula unit

observed within these minerals by EDS and microprobe analyses varies greatly (see Table 6). Variations include yttrocerite rich in La, Th, Nd, Dy, and Yb. Yttrofluorite varieties include those rich in Dy, Yb, Lu, Er, and Tm. EDS analysis identified the main REE components of the X-fluoride mineral as Ce, La and Nd. Additional REE minerals have been observed and detailed in other papers (Shannon and Goodell 1986; Rubin et al. 1987; Price et al. 1990; Hulse et al. 2013; Pingitore et al. 2014). These include aeschynite, and an unknown Nb-REE fluoride (labeled (W)-unknown).

The REE-fluorides are typically anhedral and interstitial in nature, suggesting late-stage crystallization. They form as individual crystals or in groups with multiple crystals. Their size varies but typically is ~1–40 μm, although groups of crystals have been observed to be over 100 μm in length. Yttrofluorite has been observed in several forms, including along the outer potion of feldspar phenocrysts within the K overgrowths, as inclusions to other minerals, and within the K-feldspar portion of the rhyolite groundmass (Fig. 14). Yttrocerite has been observed as individual crystals, as inclusions to other minerals, and within the groundmass of the rhyolite.

The X-fluoride mineral has only been observed as several inclusions within the same Fe-rich biotite phenocryst. Crystals varied from semi-circular to elongate in habit (Fig. 14). The size of the crystals varied from <5–10 μm in length. The REE-fluorides are typically anhedral and may range from very

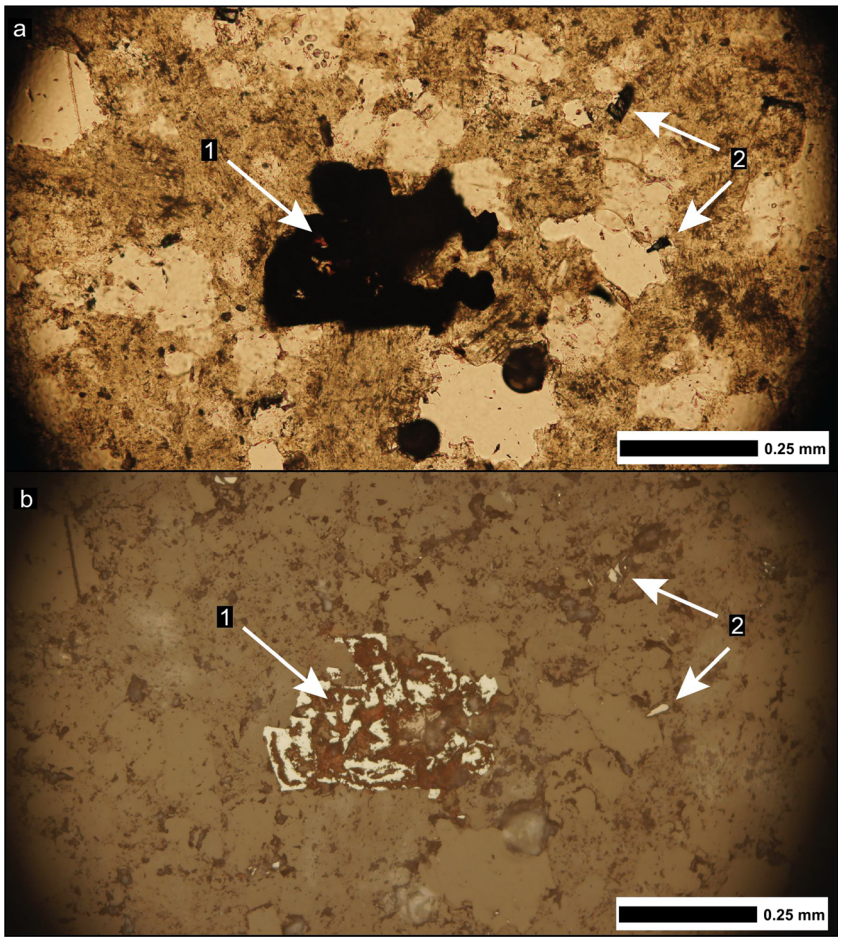

Fig. 10 Photomicrographs of a magnetite phenocryst with pock-like oxidation texture under (**a**) plane polarized light and (**b**) reflected light. Partial oxidation of magnetite phenocrysts to hematite (1) becomes more abundant when transitioning from gray, to purple, to red rhyolite. Magnetite also occurs as microcrysts within the groundmass (2)

minor constituents of the overall phenocryst to large inclusion components of the host crystal (~1–40 μm). In association with an Fe-rich biotite phenocryst, the REE-fluorides partially conform to the direction of the basal cleavage, suggesting preferential substitution and contemporaneous crystallization with the biotite (Fig. 14). When included within a quartz

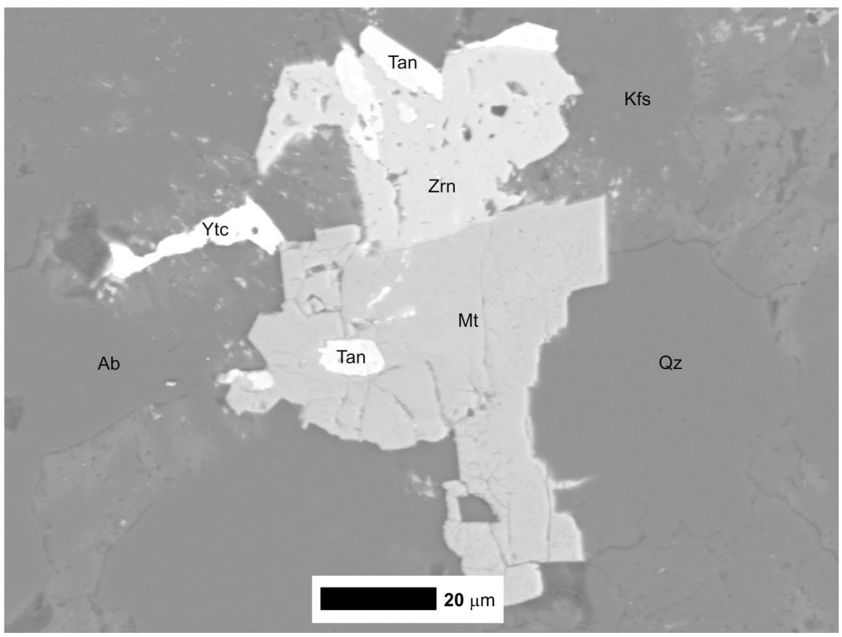

Fig. 11 BSE image of a euhedral to subhedral magnetite phenocryst (Mt) with tantalite inclusions (Tan), in close association with zircon phenocrysts (Zrn) with tantalite inclusions, and yttrocerite (Ytc). The magnetite phenocrysts commonly occur in close association with other accessory and trace mineral phases, as seen here. Note the K-feldspar (Kfs) groundmass close to the magnetite phenocryst with iron-oxide pore-fill, and the K-feldspar and plagioclase (Ab) groundmass distal to the magnetite phenocryst without pore-fill

Table 4 Quantitative EDS analyses of iron oxide minerals from the Round Top rhyolite. FeO and Fe_2O_3 calculated using charge balance

Iron Oxides												
Analysis	1	2	3	4	5	6	7	8	9	10	11	12
F	0.00	0.00	0.00	0.00	0.00	0.00	0.00	0.00	0.77	0.00	0.00	0.00
V_2O_5	0.00	1.02	0.00	0.00	0.00	0.00	0.00	0.00	0.00	0.00	0.00	0.00
SiO_2	3.99	0.00	0.00	0.00	0.00	0.00	0.00	6.05	13.7	3.18	0.00	0.00
TiO_2	1.16	1.25	0.00	0.00	0.00	0.00	1.13	0.00	0.00	0.00	0.00	0.00
Al_2O_3	3.62	0.00	3.40	0.00	3.48	0.00	0.00	0.00	0.00	0.00	0.00	0.00
Fe_2O_3	50.0	65.6	63.5	65.9	65.0	69.0	67.7	55.4	37.3	61.9	58.6	68.2
Ga_2O_3	0.00	0.00	1.37	0.00	0.00	0.00	0.00	0.00	0.00	0.00	0.00	0.00
Y_2O_3	0.00	0.00	0.00	0.00	0.00	0.00	0.00	0.00	0.00	0.00	2.27	0.75
Ce_2O_3	0.00	0.00	0.00	0.00	0.00	0.00	0.00	0.00	0.00	0.00	13.1	0.46
Lu_2O_3	0.00	0.00	0.85	0.00	0.00	0.00	0.00	0.00	0.00	0.00	0.00	0.00
CaO	0.00	0.00	0.00	0.00	0.00	0.00	0.00	0.00	0.00	0.00	1.17	0.46
MnO	0.00	0.00	0.00	1.93	0.00	0.00	0.00	0.00	0.00	0.00	0.00	0.00
FeO	31.3	32.1	30.8	27.9	31.5	31.0	31.2	38.6	48.2	34.9	24.9	30.1
ZnO	5.40	0.00	0.00	0.00	0.00	0.00	0.00	0.00	0.00	0.00	0.00	0.00
Na_2O	4.47	0.00	0.00	4.29	0.00	0.00	0.00	0.00	0.00	0.00	0.00	0.00
Total	100.00	100.00	100.00	100.00	100.00	100.00	100.00	100.00	100.00	100.00	100.00	100.00

phenocryst, the REE-fluorides may take a wide range of forms including small (<1 μm) circular inclusions to larger (>5 μm) anhedral crystals.

Cassiterite

Cassiterite (SnO_2) is one of the more abundant non-REE-bearing trace phases, although Nb_2O_5 ranges from 7.82–9.59% (see Table 5), and is less common than some of the other trace phases, such as columbite and changbaiite. It most commonly occurs as inclusions and in close association with other accessory phases (Fig. 15). Phenocrysts are typically subhedral to anhedral and range from small inclusions (≤5 μm) to relatively large crystals (50 μm). The contact edges of the cassiterite and adjacent crystals are typically irregular and embayed.

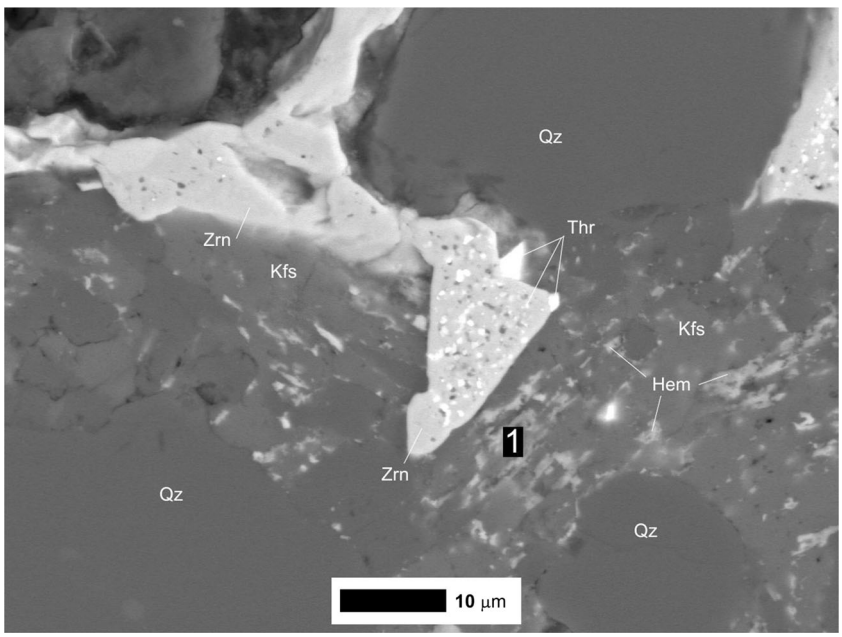

Fig. 12 BSE image of hematite (Hem) pore-fill within the K-feldspar (Kfs) groundmass. The iron oxide appears as *medium gray* wispy inclusions within the *darker gray* K-feldspar groundmass (1). These inclusions has only been observed within the K-feldspar portion of the groundmass and is believed to be the cause of the turbid texture of the rhyolites. The hematite pore-fill is not pervasive throughout the groundmass, but rather occurs as patches, typically associated with other trace and accessory phases

Table 5 Quantitative EDS analyses (wt% oxide) of zircon, cassiterite, and changbaiite from the Round Top rhyolite

Zircon							Cassiterite			
Analysis	1	2	3	4	5	6	Analysis	1	2	3
SiO_2	33.9	36.2	37.0	36.4	36.1	35.1	Nb_2O_5	9.59	7.82	7.82
ZrO_2	52.7	62.8	58.7	58.3	62.5	57.1	SiO_2	5.12	6.32	6.32
HfO_2	0.00	0.00	1.45	5.34	1.45	5.20	TiO_2	0.49	0.80	0.80
ThO_2	2.37	0.00	0.00	0.00	0.00	0.80	SnO_2	75.8	81.6	81.6
UO_2	1.51	0.00	2.93	0.00	0.00	1.81	Al_2O_3	1.77	0.00	0.00
Al_2O_3	2.06	0.00	0.00	0.00	0.00	0.00	MnO	1.17	0.39	0.39
OsO	7.48	0.00	0.00	0.00	0.00	0.00	FeO*	4.80	3.07	3.07
K_2O	0.00	0.95	0.00	0.00	0.00	0.00	Na_2O	1.22	0.00	0.00
Total	100.00	100.00	100.00	100.00	100.00	100.00	Total	100.00	100.00	100.00
Changbaiite										
Analysis	1	2	3	4	5	6	7	8	9	10
F	0.00	1.71	0.00	0.00	1.92	0.00	2.48	0.00	0.61	5.97
Nb_2O_5	10.9	15.4	14.7	13.7	10.5	11.3	12.0	14.0	9.60	10.2
Ta_2O_5	0.00	0.00	0.00	0.00	5.14	4.51	0.00	0.00	7.83	0.00
SiO_2	5.55	5.80	7.56	3.21	5.66	5.37	5.44	6.45	9.32	4.35
TiO_2	1.44	0.00	0.00	0.21	0.00	2.10	0.00	0.00	0.28	0.72
SnO_2	3.48	0.00	0.00	0.00	0.00	0.00	0.00	0.00	0.00	0.00
PbO_2	73.8	73.7	65.5	77.0	71.2	75.1	70.2	73.5	69.4	64.0
Al_2O_3	1.52	0.00	2.80	0.51	0.00	0.00	3.07	1.89	0.00	1.55
Y_2O_3	0.00	0.00	1.02	2.08	0.00	0.00	0.00	0.00	0.00	4.87
Dy_2O_3	0.00	0.00	5.69	0.00	0.00	0.00	0.00	0.00	0.00	3.43
Ho_2O_3	0.00	0.00	0.00	0.00	3.10	0.00	0.00	0.00	0.00	0.00
Tm_2O_3	0.00	0.00	0.00	0.00	0.00	0.00	0.00	0.00	0.00	0.00
MgO	0.00	0.00	0.00	0.00	0.00	0.00	1.82	0.00	0.00	0.00
MnO	0.00	0.00	0.00	0.36	0.00	0.00	0.00	0.00	0.26	0.00
FeO*	3.24	3.40	2.76	2.94	2.49	1.66	2.57	4.15	2.69	2.02
CaO	0.00	0.00	0.00	0.00	0.00	0.00	1.28	0.00	0.00	2.10
Na_2O	0.00	0.00	0.00	0.00	0.00	0.00	1.17	0.00	0.00	0.82
Total	100.00	100.00	100.00	100.00	100.00	100.00	100.00	100.00	100.00	100.00

Cerianite

Cerianite [$(Ce,Th)O_2$] occurs as inclusions within the K-feldspar-rich portions of the rhyolite groundmass. The crystals are anhedral and range from <1–5 μm in diameter. The cerianite occurs in clusters, conforming to pore-spaces in the groundmass, indicating formation during late-stage hydrothermal activity. Additionally, the edges of the cerianite are

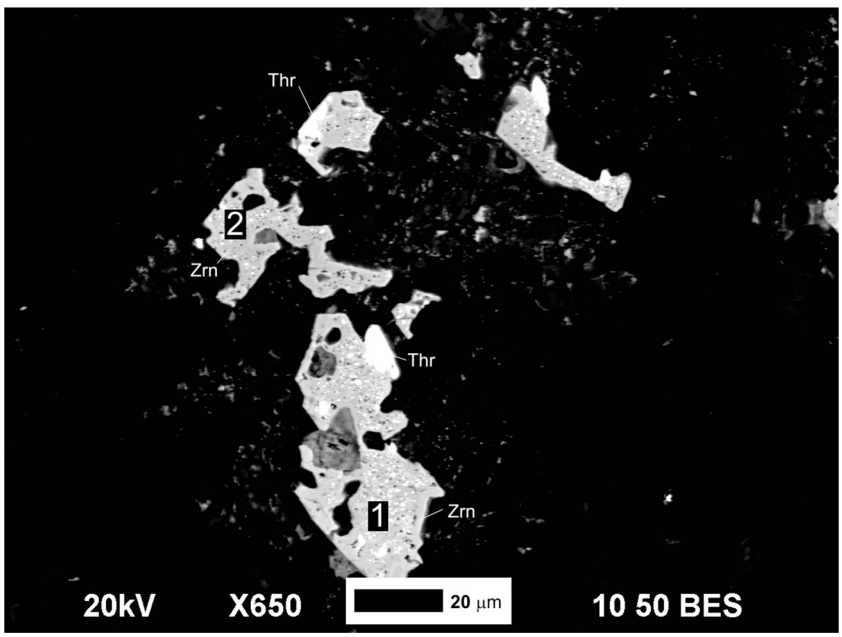

Fig. 13 BSE image of a cluster of subhedral and anhedral zircon phenocrysts (Zrn). Euhedral to subhedral zircon phenocrysts (1) are rare. Typically, the zircons are anhedral (2) and display amoeboid-like morphologies with abundant embayments and thorite (Thr) overgrowths. All of the zircons featured contain abundant thorite inclusions

Table 6 Quantitative EDS analyses (wt% oxide) of fluorite from the Round Top rhyolite

Fluorite								
Analysis	1	2	3	4	5	6	7	8
F	32.3	35.4	32.6	34.0	30.2	28.2	27.4	40.1
Ta_2O_5	0.00	0.00	0.00	0.00	2.31	0.00	0.00	0.00
SiO_2	3.02	3.30	1.38	0.00	0.00	5.80	12.3	2.53
Al_2O_3	5.61	2.07	3.19	0.00	0.00	6.77	0.00	2.39
Y_2O_3	29.9	33.5	30.3	36.9	32.4	31.9	23.2	23.0
Ce_2O_3	0.00	0.00	0.00	0.00	0.00	0.00	6.22	9.04
Nd_2O_3	0.00	0.00	0.00	0.00	0.00	0.00	3.60	0.00
Dy_2O_3	7.01	0.00	0.00	5.02	4.32	6.48	3.52	0.00
Er_2O_3	0.00	0.00	0.00	4.11	2.33	0.00	4.40	0.00
Tm_2O_3	0.00	0.00	0.00	0.95	0.00	0.00	0.00	0.00
Yb_2O_3	0.00	5.15	4.29	0.00	10.8	0.00	3.10	0.00
Lu_2O_3	0.00	0.00	7.59	0.00	0.00	0.00	0.00	0.00
CaO	12.0	10.0	10.9	9.9	11.5	12.8	8.96	17.0
MnO	0.00	0.74	0.00	0.00	0.00	0.00	0.00	0.00
FeO*	0.00	0.00	0.58	0.44	0.00	0.00	0.00	0.00
Na_2O	10.0	9.23	8.59	8.68	6.08	6.82	7.22	5.97
K_2O	0.00	0.59	0.53	0.00	0.00	1.17	0.00	0.00
Total	100.00	100.00	100.00	100.00	100.00	100.00	100.00	100.00

commonly apophysial or tail-like, conforming to the surrounding quartz and groundmass crystals. This relation suggests the cerianite and the groundmass formed contemporaneously and/or the cerianite filled in pore spaces and fractures at a later stage.

Changbaiite

Changbaiite ($PbNb_2O_6$) occurs as fracture fill, along grain boundaries, and as inclusions in other accessory phases, including columbite and magnetite (Fig. 16). The crystals are typically anhedral and range from 5 to 10 μm in diameter. The inclusions of changbaiite are dispersed throughout and along the outer edges the host phenocryst. When the changbaiite occurs along microfractures and along grain boundaries, the crystals conform to the adjacent phenocrysts and groundmass, suggesting concurrent or late-stage crystallization. Microprobe analyses of changbaiite show variable Y and REE content, including Dy, Tm, and Ho (see Table 5).

Columbite and tantalite

Columbite ($FeNb_2O_6$) and tantalite [$(Fe,Mn)(Ta,Nb)_2O_6$] typically occur in close association with other accessory

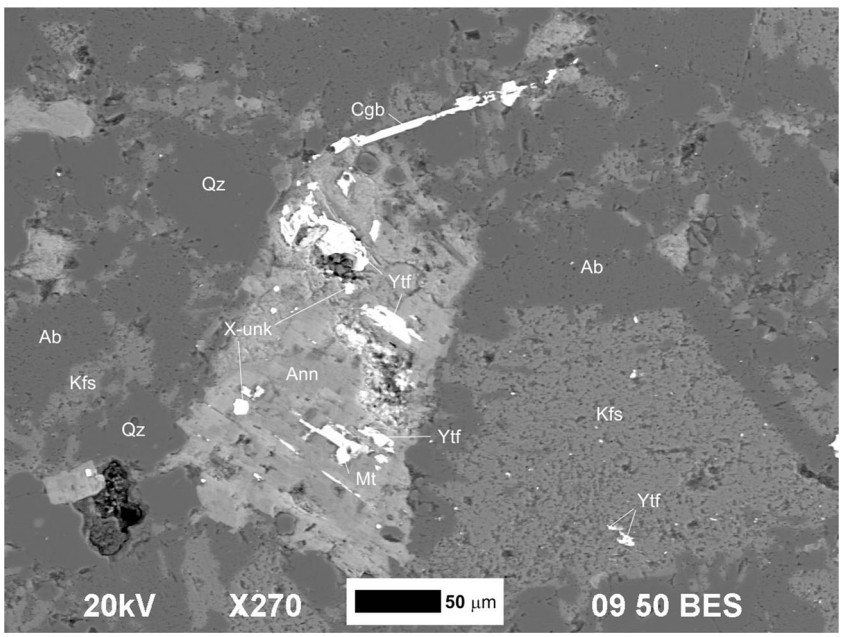

Fig. 14 BSE image of an annite phenocryst with multiple mineral inclusions. The inclusions include yttrofluorite (Ytf), magnetite (Mt), and unidentified X-fluoride (X-unk). REE-inclusions typically partially conform to the direction of the biotite basal cleavage. Changbaiite (Cgb) is visible in close association with the Fe-rich biotite phenocryst (Ann), as is multiple yttrofluorite inclusions within the adjacent K-feldspar (Kfs) phenocryst

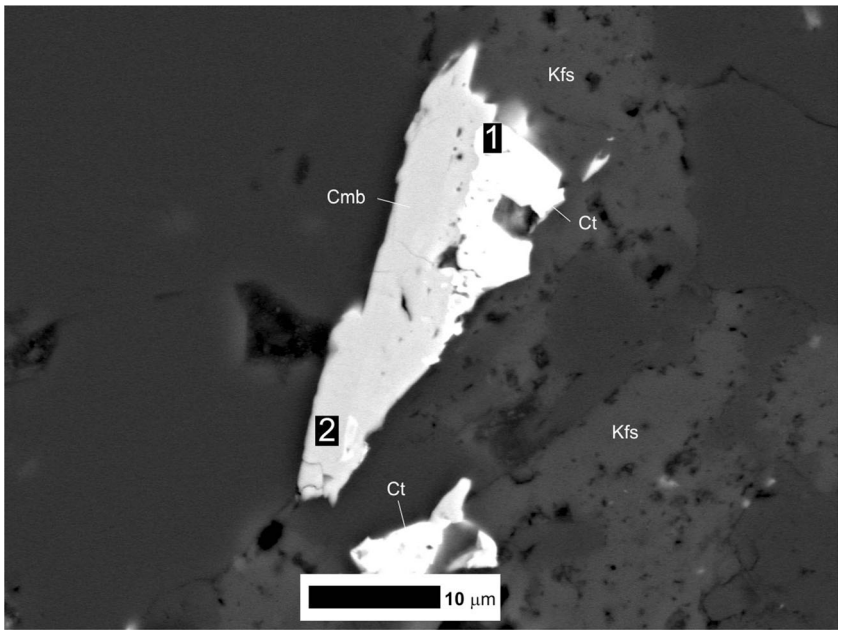

Fig. 15 BSE image of late-stage intergrown cassiterite (Ct) and columbite (Cmb) crystals. Note the undulatory boundary between the two grains (1) and the inclusion of cassiterite within the columbite (2) representing concurrent crystallization. The trace phases are interstitial to the other crystals and within the K-feldspar (Kfs) portion of the groundmass. The brightness and contrast settings have been turned down in order to be able to see the mineral relationship

phases, including magnetite, cassiterite, and changbaiite. Compositionally, most analyzed grains are classified as ferro-columbite, with a few analyses extending into the mangano-columbite field (see Fig. 17). Columbite-tantalite mineralization is predominantly niobium enriched with Ta/(Ta + Nb) ranging from 0.00 to 0.12 (see Table 7). Of the trace phases, columbite is the most abundant, and typically displays the largest crystals. Crystals are subhedral to anhedral and range from 20 to 120 μm in length. Columbite commonly contains inclusions of other trace phases, particularly cassiterite and changbaiite. The contacts between the inclusions and the host columbite are embayed and irregular. Tantalite inclusions in the groundmass commonly conform to the surrounding grain boundaries, forming tail-like apophyses in thin section. This close association to other accessory and trace phases in the groundmass suggests late-stage crystallization in the paragenetic sequence.

Cryolite

Only two crystals of cryolite (Na_2NaAlF_6) were observed in the sample examined Each occurred as an inclusion within the

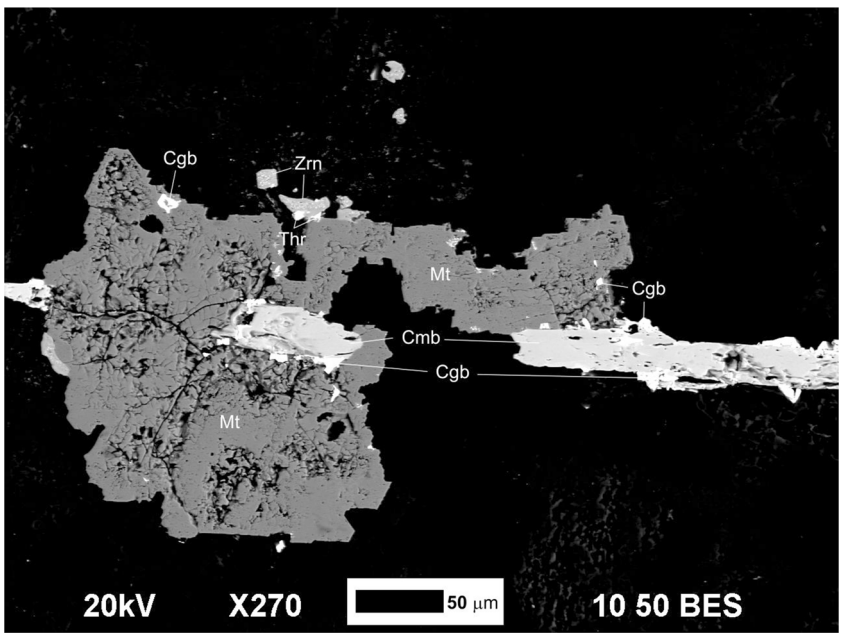

Fig. 16 BSE image of intergrown changbaiite (Cgb) and columbite (Cmb) phenocrysts. The intergrown changbaiite and columbite are inclusions within a magnetite (Mt) phenocryst and adjacent to thorite-rich (Thr) zircons (Zrn). The intermingled nature of the phenocrysts suggests that crystallization of the mineral suite was contemporaneous

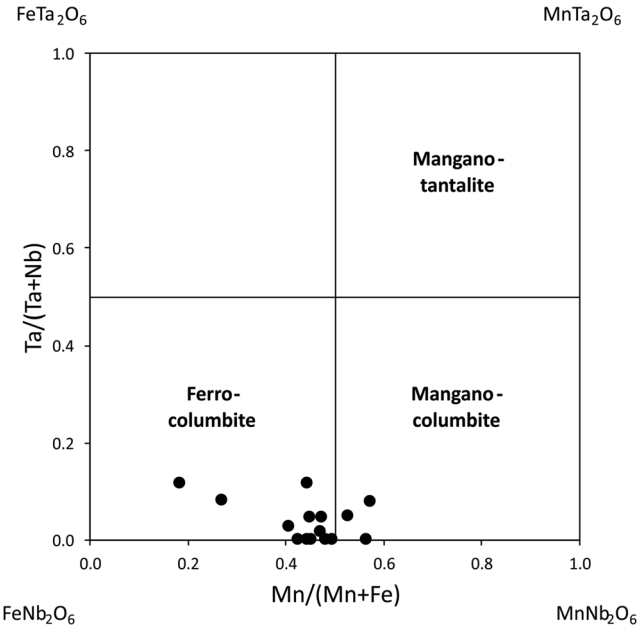

Fig. 17 Classification of columbite ($FeNb_2O_6$) and tantalite [$(Fe,Mn)(Ta,Nb)_2O_6$] minerals from the Round Top rhyolite

K-feldspar portion of the rhyolite groundmass, in close proximity to each other in the same sample. The inclusions are anhedral and thin, with a total width of <1 μm. EDS analyses indicated an anomalous enrichment of Ca within either cryolite crystal. The surrounding plagioclase and K-feldspar groundmass is known to be depleted in Ca, so it is unlikely this is an overlapping signal from the surrounding minerals, and possibly an indication of fluorite produced through late-stage alteration. The anhedral shape of the inclusions and their occurrence within the groundmass suggests late-stage crystallization, either contemporaneous to, or subsequent to the formation of the groundmass.

Thorite

Thorite [$Th(SiO_4)$] occurs as inclusions within zircon phenocrysts, and as individual crystals within the K-feldspar portion of the groundmass. In both populations, the thorite is anhedral and irregular in shape. The size of the thorite varies greatly from <1–10 μm in diameter. When many crystals occur in close proximity, the variation in size may be great. The thorite inclusions within the zircon phenocrysts indicate contemporaneous formation and/or exsolution of the thorite from the zircon. The occurrence of thorite along the grain boundaries and within fractures suggests either concurrent or subsequent crystallization of the thorite in the groundmass. Thorite compositions are highly variable depending on the location of the inclusions, but U and Th concentrations are relatively homogenous (see Table 7).

Table 7 Quantitative EDS analyses (wt% oxide) of columbite and thorite from the Round Top rhyolite

Columbite													Thorite			
Analysis	1	2	3	4	5	6	7	8	9	10	11	12	Analysis	1	2	3
F	0.00	0.00	0.00	0.00	0.00	0.00	5.13	3.64	0.00	0.00	0.00	1.72	F	3.96	3.52	0.00
V_2O_5	0.00	0.00	0.00	0.00	0.00	0.00	0.00	0.00	0.00	1.05	0.00	0.00	P_2O_5	0.00	3.21	0.00
Nb_2O_5	51.9	69.7	65.1	71.3	65.6	50.2	63.3	58.5	67.7	69.2	70.1	68.6	V_2O_5	0.00	0.66	6.00
Ta_2O_5	17.2	5.03	8.55	2.67	8.19	11.4	0.00	0.00	0.00	0.00	0.00	0.00	SiO_2	11.3	29.6	17.3
Ho_2O_3	0.00	0.00	0.00	0.00	0.00	0.00	0.00	2.66	0.00	0.00	0.00	0.00	ZrO_2	17.7	0.00	14.4
SiO_2	13.5	6.07	6.25	4.07	7.92	12.7	10.2	3.23	2.65	6.17	4.01	4.22	ThO_2	42.5	41.2	41.5
TiO_2	1.20	0.00	1.33	0.00	0.00	0.00	0.00	0.00	1.96	1.45	0.00	1.30	UO_2	11.7	12.07	10.9
ZrO_2	0.00	0.00	0.00	0.00	0.00	0.00	0.00	0.00	1.63	0.00	0.00	0.00	Al_2O_3	6.04	4.12	7.48
SnO_2	0.00	0.00	0.00	0.00	0.00	0.00	0.00	0.00	0.00	0.00	0.00	2.18	CaO	2.47	1.72	1.90
PbO_2	0.00	0.00	0.00	0.00	0.00	0.00	0.00	13.2	0.00	0.00	0.00	0.00	MgO	3.23	1.88	0.00
Al_2O_3	0.00	0.00	0.00	2.23	0.00	0.00	0.00	2.01	0.56	0.00	0.00	0.00	MnO	0.00	0.00	0.53
Y_2O_3	0.00	0.00	0.00	0.00	0.00	0.00	0.00	0.00	4.78	0.00	0.48	0.00	FeO*	1.14	0.00	0.00
Dy_2O_3	0.00	0.00	0.00	0.00	0.00	0.00	0.00	0.00	0.00	0.00	9.70	0.00	Na_2O	0.00	1.95	0.00
MnO	7.16	7.78	9.86	9.26	8.60	6.82	9.03	8.28	9.28	9.31	8.85	10.1	Total	100.00	100.00	100.00
FeO*	9.01	11.4	8.89	10.5	9.65	18.8	12.4	8.55	11.4	11.8	6.85	11.1				
CaO	0.00	0.00	0.00	0.00	0.00	0.00	0.00	0.00	0.00	1.01	0.00	0.00				
K_2O	0.00	0.00	0.00	0.00	0.00	0.00	0.00	0.00	0.00	0.00	0.00	0.80				
Total	100.00	100.00	100.00	100.00	100.00	100.00	100.00	100.00	100.00	100.00	100.00	100.00				
Mn/(Mn + Fe)	0.45	0.41	0.53	0.47	0.47	0.27	0.43	0.50	0.45	0.44	0.57	0.48				
Ta/(Ta + Nb)	0.12	0.03	0.05	0.01	0.05	0.08	0.00	0.00	0.00	0.00	0.00	0.00				

Nb-rich oxides

Nb-rich oxides are present and have minor amounts of Ta, Fe, Mn, Pb, and F. Only one occurrence of an unknown Nb-oxide mineral was identified in this study, and occurred in close proximity to two changbaiite inclusions in the groundmass. The unknown Nb-oxide mineral is anhedral and approximately 10 μm in length. Tail-like apophyses and grain morphology is similar to tantalite and other accessory phases, suggesting late-stage paragenesis.

Discussion

General remarks

Round Top is the one of the last emplaced laccoliths in the SBC. The parent magma underwent an extensive process of fractionation and elemental enrichment (Y + REE, F, U/Th, and Be), facilitated by a long-lived extensional tectonic regime.

Round Top consists of four intermingled rhyolite types that vary in color, but only slightly in mineralogy, texture, and alteration history. All rhyolite types are weakly to strongly peraluminous and subalkaline, and have undergone varying degrees of oxidation. The variations observed in the mottled textures and rhyolite colors are the product of incomplete oxidation of the laccolith by secondary fluids. These variable colorations are due to differing proportions of hematite within the pore spaces of the K-feldspar groundmass. The hematite was sourced from the oxidation of magnetite within the rhyolite and was subsequently deposited within the open pore spaces of the feldspar produced by early dissolution, or hematite alteration of the magnetite inclusions. The tan color variation has been locally subjected to intense alteration that converted the K-feldspar to clay. It is unclear what type, or types, of rhyolite the tan variation was prior to being altered.

Petrographic and microbeam studies indicate early, middle, and late stages of crystallization, followed by alteration by a high temperature vapor phase and subsequent oxidization. The Round Top rhyolite mineral modes are 48–52% K-feldspar, 28–30% quartz, 8–14% plagioclase, 4–5% Fe-rich biotite, 2–3% magnetite-hematite, 1% zircon and other trace phases, including Y + REE-fluoride minerals. The trace phases include tantalite, columbite, cerianite-(Ce), thorite, changbaiite, cryolite, cassiterite, yttrocerite, yttrofluorite, Ca-Th-Pb fluorides, and Nb-rich oxides.

Magma evolution and emplacement

The specific conditions necessary to form a REE-enriched deposit in highly evolved subalkaline rhyolites have not been well documented. The peraluminous composition of the Round Top rhyolite differs from many of the more peralkaline and metaluminous rhyolites within the Trans-Pecos region, suggesting a difference in the formation process or timing of emplacement (Barker 1980; Rubin et al. 1987; Price et al. 1990).

Regional magmatism and timing between tectonic events were favorable for a continentally sourced, highly differentiated silicic magma to evolve at depth and be emplaced in a relatively shallow environment. The complex tectonic history of the Trans-Pecos region has played a key role in the development of this magmatic source, providing heat and hosting early mafic to intermediate magmatic episodes. The periodic compressive events, punctuated by abrupt stress orientation changes and subsequent regional extension, and overprinted with multiple generations of faulting and volcanism, created a geologic setting favorable to episodic isothermal fractionation and prolonged differentiation (see London 2014).

To form the laccolith structure, magmatic material stalled during ascension, extended laterally, and was prevented from erupting at the surface. The entrapment of the magma within the Cretaceous strata was controlled by buoyancy and density contrasts between the Cretaceous overburden and the upwelling silicic magma. The high F content and volatile-rich nature of the magma additionally contributed to the stalling of the igneous material by altering the viscosity of the igneous fluids. Fluorine, as with water, has been identified as a mechanism to decrease the viscosity of volatile-rich silicic magmas (Giordano et al. 2004; Vernon 2004). The SBC is a hypabyssal intrusive complex, with possible upper "cupola" portions of the laccolith structures and evidence of contemporaneous volcanism lost to erosion. The convex shape and dome peaks that characterize the group suggest an emplacement of moderate force, causing mild deformation of the surrounding rocks as the magma pooled and uplifted the overlying strata. Crystallization of the magma began at depth, forming large euhedral phenocrysts of alkali feldspar, quartz, and plagioclase. Subsequent fractionation processes continued to differentiate the magma, where episodic isothermal decompression events caused dissolution of alkali feldspar and recrystallization as mantles on plagioclase phenocrysts (e.g. similar processes of feldspar and quartz resorption/recrystallization detailed in Muller et al. 2008, 2009). The groundmass nucleated and crystallized quickly, as evidenced by undercooling textures (e.g. Hammer and Rutherford 2002). Pore spaces in the groundmass and late-stage vapor phase mineralization suggests a late- to post-magmatic hydrothermal overprint. The enclosing Cretaceous strata would have produced an ideal environment to trap residual magmatic volatiles, thus facilitating rapid quenching and crystallization of the groundmass. As the laccolith cooled, the vapor phase formed late-stage trace phases and REE-fluorides. Crystallization of the laccolith as a whole was relatively rapid, as the rhyolite is uniformly aphanitic.

Post-magmatic fluid migrated along fractures, and within the rhyolitic body, oxidizing portions of the laccolith. Fluid-mineral interaction caused the magnetite phenocrysts to

oxidize, producing abundant hematite. The color variation in the rhyolite is the product of increasing proportions of hematite, primarily within the micropores of the alkali feldspar groundmass. The origin of the more highly geometric mottled textures is potentially related to microfractures and joints within the rhyolite. Mineralization and cementation of fractures and joints within the laccolith are common, producing multiple generations of fluorite, calcite, and microcrystalline silica. The ubiquitous mineralization is suggestive of a prolonged period of remobilization and precipitation, facilitated by circulating oxidizing fluids.

Emplacement and rhyolite textures

The Round Top magma was emplaced into thinly bedded Cretaceous strata, relatively contemporaneous with the formation of the adjacent laccoliths of the SBC, circa 36 Ma (Henry and McDowell 1986). With continued injection, the magmatic body increased in volume displacing the overlying strata. This emplacement style formed the domed convex structure currently observed. The undulatory and irregular basal contact between the laccolith, Cretaceous strata, and diorite sill suggest the magma was injected along bedding planes at multiple depths. The rhyolitic magma most likely utilized the preexisting conduit of the diorite sill during emplacement, although enclaves of the preexisting mafic sill have not been documented within the rhyolite.

The abundance of disequilibrium textures and the anhedral morphology of groundmass mineralogy throughout the laccolith suggest rapid crystallization. The hourglass sector zonation of the K-feldspar phenocrysts is an uncommon disequilibrium texture that occurs as a result of preferential site allocation of Na and K during formation, indicating rapid crystallization and growth during disequilibrium (Shelley 1992; Vernon 2004). Additionally, the euhedral outer edge of many of the interior plagioclase laths and interior quartz cores indicate that corrosion of the phenocrysts did not occur until after the formation of late-stage overgrowths. The three-part quartz phenocrysts indicate a transition from conditions favoring euhedral high-temperature beta quartz formation to more rapid crystallization of low-temperature quartz, entraining magmatic material in the form of melt inclusions. The uniform occurrence of these disequilibrium textures throughout all of the rhyolite types suggests that the change in pressure-temperature conditions affected the entirety of the laccolith, and it is unlikely that the laccolith was emplaced in multiple magmatic events.

The highly fractured nature of the laccolith allowed the movement of the primary and secondary fluids responsible for alteration and oxidation, as evident by the abundance of rhyolite and host-rock breccia and cemented fractures. These fractures are the result of rapid cooling and subsequent shrinking of the laccolith after emplacement. Later Basin and Range extension probably contributed to the continued faulting and jointing of the laccolith.

Timing and crystallization of REE-enriched minerals

The petrogenetic sequence of the Round Top laccolith includes early, middle, and late crystallization phases, which were subjected to late-stage alteration from a volatile-rich vapor phase and post-magmatic partial oxidation from circulating fluids (Fig. 18). Given the observed mineralogical relationships between the major, accessory, and trace phases, early crystallization included the formation of the larger phenocrysts within the magma chamber and progressed through emplacement. Crystallization and alteration ceased with the quenching of the vapor phase. During the final stages of crystallization, interaction with the volatile-rich, vapor phase produced the alteration textures now observed within the feldspars and quartz overgrowths. Interaction with post-magmatic oxidizing fluids partially altered the laccolith to form color variations and mottled rhyolite types. Crystallization of the major phases began within the magma chamber, forming the plagioclase feldspar laths (that would later become the cores to the larger feldspar phenocrysts), and the hexagonal, higher temperature core portions of the quartz phenocrysts. Emplacement of the magma from depth to the current stratigraphic position within the Cretaceous strata was relatively rapid, which inhibited significant crystallization during transport as evidenced by the fine grained and uniform nature of the groundmass. During the emplacement of the laccolith, as temperature and pressure conditions decreased, the subhedral to euhedral, hourglass-type K-feldspar phenocrysts, the K-feldspar overgrowths, the smaller accessory phases, and the larger constitutes of the groundmass (K-feldspar, plagioclase, quartz, and annite) began to crystallize. Interaction of these minerals with the circulating high temperature volatile-rich vapor phase produced the dissolution textures observed in feldspar and quartz. This late magmatic phase is partly characterized by a process that liberates Nb, Ta, Sn, and W, subsequently crystallizing cassiterite, columbite tantalite, and other Nb-enriched phases. As new magma ceased to be emplaced and the laccolith cooled, the volatile-rich vapor phase quenched to form the accessory, late-stage phases. These late-stage phases occur interstitial to and within the K-feldspar pores, and include cerianite-(Ce), columbite, tantalite, changbaiite, cassiterite, yttrocerite, yttrofluorite, and the X-fluoride and other Nb-oxide minerals. The intimate association of the REE-fluoride minerals and other trace phases with the magnetite, zircon, and groundmass, suggests that the timing of crystallization between all phases was relatively close. The skeletal corrosion textures and REE-fluoride minerals may be intimately connected through the reaction 2(REE)OF +

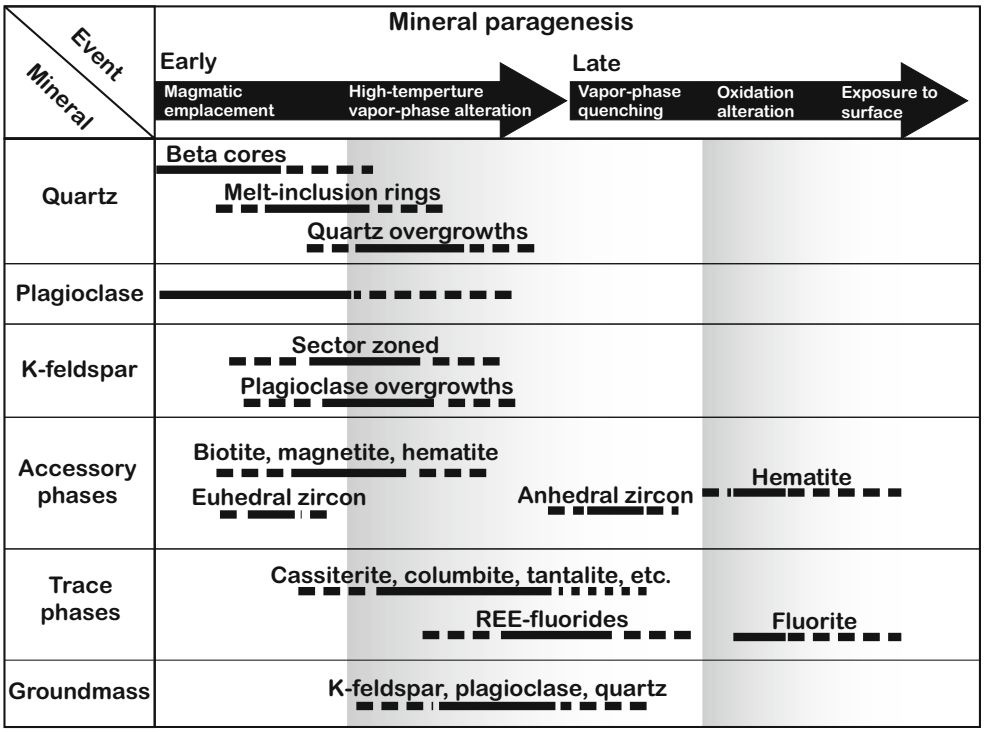

Fig. 18 Paragenetic sequence of the crystallization and alteration of the Round Top rhyolite laccolith minerals

$H_2O \rightarrow (REE)_2O_3 + 2HF$, precipitating REE-bearing minerals and increasing f_{HF} (cf. Zachariansen 1951; Johan and Johan 2005).

The different stages of crystallization and subsequent alteration by the vapor phase must have occurred with a high degree of overlap and within a relatively short duration, as evident by the many inclusions of different mineral phases from one stage within another. The emplacement of the magma body would have rapidly shifted the pressure and temperature conditions of the system, causing disequilibrium growth and subsequent mantling of the plagioclase by the K-feldspars and the quartz overgrowths. The abundance of volatiles within the vapor phase potentially acted to buffer the formation of crystals until later within the petrogenetic sequence, as is observed in other systems with abundant F and Li (Vernon 2004). The partial oxidation of portions of the laccolith occurred subsequent to the quenching of the vapor phase, as redox conditions changed during ascent, degassing and final emplacement (e.g. Burgisser and Scaillet 2007), but prior to exhumation of the laccolith.

Rubin et al. (1989a, b; 1993) suggested that the two zircon populations of the Round Top rhyolite (thorite-rich and thorite-poor) indicate dissolution and recrystallization of a portion of the zircons during subsequent hydrothermal alteration of the laccolith. This is unlikely given the nature of fluid that would be necessary to conduct such selective remobilization. It is unclear as to how an acidic fluid (such as those associated with hydrothermal alteration and with the acidity necessary to dissolve zircon), could preferentially dissolve zircon while not dissolving adjacent quartz, K-feldspar, and plagioclase phenocrysts. Therefore, the two populations of zircon most likely represent one population that is in varying stages of thorite exsolution (c.f. Lisowiec et al. 2012).

Alteration – Color and textural variations in rhyolite

At the time of crystallization and just subsequent to, the laccolith was subjected to a relatively uniform degree of alteration prior to undergoing oxidation. This alteration caused the partial dissolution and formation of the semi-linear pores spaces within the K-feldspar phenocrysts, overgrowths, and feldspar groundmass, in addition to forming the embayments of quartz overgrowths. Dissolution of the feldspars must have occurred prior to the crystallization of the late-stage minerals in order to produce the inclusionary relationship observed between the two groups. The strong correlation between the REE-minerals and the K-feldspar in the rhyolite suggests the availability of open pore space was a significant factor in the retention of the REE-fluorides. This close mineralogical relationship should therefore be considered in future economic investigations. The ubiquitous nature of the quartz embayment and feldspar dissolution suggests that vapor phase alteration was pervasive throughout the entirety of the laccolith.

The depletion in REE, the kaolinization of the K-feldspar, and the localized occurrence of the tan rhyolite suggest that this limited portion of the laccolith was subjected to a form of alteration different to that of the rest of the laccolith, and may be due to prolonged interaction with late acidic hydrothermal fluids.

Conclusions

The Round Top laccolith represents the last magmatic emplacement of a highly evolved magmatic system, enriched in incompatible elements including REE, U, Be, Nb, Ta, and F. Conclusions regarding the magmatic evolution and elemental enrichment of the Round Top laccolith are as follows: (i) The high temperature mineral-vapor phase alteration of the feldspar groundmass, along with increasing f_{HF}, was essential to the formation of REE minerals, where the pervasive open pore space was occupied by late-crystallizing F-complexing minerals. These late-forming REE-bearing minerals also occur as crystals associated with other accessory and trace phases, as inclusions within other late phases, along phenocryst grain boundaries, along fractures and within voids. (ii) Differences in fluorite content between rhyolite color varieties represent innate heterogeneity in the concentration of the volatile-rich vapor phase at the time of crystallization. (iii) There are many textural and color variations in the rhyolite and the occurrence of mottled rhyolite textures are the product of selective alteration produced by the migration of oxidizing fluids. Gray rhyolite represents the rock type that has had the least interaction with these oxidizing fluids, whereas the red represents that which has had the most).

The REE enrichment in the Round Top rhyolite is the result of the prolonged removal of compatible elements from source magma chamber through the emplacement of earlier magmatic events. With the emplacement of each sequential laccolith, the source magma became more enriched in incompatible elements, evident by the associated increasing REE concentrations. The emplacement of Round Top as a laccolith (versus that of an extrusive rhyolitic flow) facilitated the retention of a volatile-rich vapor phase within the magma, allowing for the formation of abundant REE-minerals. Additionally, the retention of a high temperature vapor phase produced the pores and inclusions within the feldspars, creating the necessary space occupied by the quenched volatile phase. Recognizing highly evolved REE-enriched magmatic systems similar to that of Round top should help focus on identifying non-traditional regions and igneous suites that have REE-mineral potential. These intrusions will be situated within long-lived, complex tectonic regimes that have been subjected to regional compression and subduction, punctuated by extensional bimodal volcanism and prolonged differentiation before emplacement. Felsic volcanic centers not yet exposed at the surface, possibly less affected by remobilizing secondary oxidation and erosion, may be present in other regions and not identified as having REE resource potential.

Acknowledgements We thank the Texas Rare Earth Resources Corporation for permission to conduct research on their property, assistance in conducting fieldwork, and providing access to existing maps, drill-hole data and samples, and previous studies. We are indebted to two anonymous experts as well as editor Daniel Harlov whose critical and constructive reviews helped to greatly improve the manuscript's overall content and quality. The funding for this study was provided by the Jackson School of Geosciences and the State of Texas Advanced Resource Recovery (STARR) program through the University of Texas at Austin, Bureau of Economic Geology, Mineral Resource Program. This study was greatly enhanced by regional mapping products, produced by the University of Texas at Austin Bureau of Economic Geology, and funded through the United States Geological Survey Mapping Cooperative Program, STATEMAP Award No. G13AC00178. Additional support for O'Neill (2014) thesis research was provided by the III Yager Professorship of the Jackson School of Geosciences, the West Texas Geological Society, the Society of Economic Geologists, and the Association of Environmental and Engineering Geologists.

References

Albritton CC Jr, Smith JF Jr (1965) Geology of the Sierra Blanca area, Hudspeth County, Texas. Geol Surv Prof Pap, vol 479. US Geol Surv, Washington DC, 131 pp

Barker DS (1977) Northern Trans-Pecos magmatic province: introduction and comparison with the Kenya rift. Geol Soc Am Bull 88(10): 1421–1427

Barker DS (1979) Magmatic evolution in the Trans-Pecos province. In: Walton AW, Henry CD (eds) Cenozoic geology of the Trans-Pecos volcanic field of Texas. Bureau of Economic Geology, University of Texas at Austin, Guidebook 19, pp 4–9

Barker DS (1980) Cenozoic igneous rocks, Sierra Blanca area, Texas. In: Dickenson PW, Hoffer JM, Callender JF (eds) Trans-Pecos region, southeastern New Mexico and West Texas. New Mexico Geol Soc Guidebook, 31st Field Conference, pp 219–223

Barker DS (1987) Tertiary alkaline magmatism in Trans-Pecos Texas. In: Fitton JG, Upton BGJ (eds) Alkaline igneous rocks, vol 30. Geol Soc London Spec Pub, pp 415–431

Boynton WV (1984) Geochemistry of the rare earth elements: meteorite studies. In: Henderson P (ed) Rare earth element geochemistry. Elsevier, Amsterdam, pp 63–114

Burgisser A, Scaillet B (2007) Redox evolution of a degassing magma rising to the surface. Nature 445:194–197

Corry CE (1988) Laccoliths; mechanics of emplacement and growth. Geol Soc Am Spec Pap, vol 220. Geological Soc Am, Boulder, 114 pp

Giordano D, Romano C, Dingwell DB, Poe B, Behrens H (2004) The combined effects of water and fluorine on the viscosity of silicic magmas. Geochim Cosmochim Ac 68(24):5159–5168

Hammer JE, Rutherford MJ (2002) An experimental study of the kinetics of decompression-induced crystallization in silicic melt. J Geophys Res 107(B1):1–24

Henry CD, McDowell FW (1986) Geochronology of magmatism in the Tertiary volcanic field, trans-Pecos Texas. Bureau of Economic Geology, University of Texas at Austin, guidebook no 23:99–122

Henry CD, Price JG (1984) Variations in caldera development in the Tertiary volcanic field of trans-Pecos Texas. J Geophys Res 89(B10):8765–8786

Henry CD, Price JG, James EW (1991) Mid-Cenozoic stress evolution and magmatism in the southern Cordillera, Texas and Mexico; transition from continental arc to intraplate extension. J Geophys Res 96(B8):13

Henry CD, Price JG, Miser DE (1989) Geology and tertiary igneous activity of the Hen Egg Mountain and Christmas Mountains quadrangles, Big Bend region, Trans-Pecos Texas. Bureau of Economic Geology, University of Texas at Austin, Report of investigators, vol 183, 105 pp

Hulse DE, Newton MC III, Malhotra D (2013) NI 43–101 preliminary economic assessment, Round Top project, Sierra Blanca, Texas. Texas Rare Earth Resources Corp, Sierra Blanca, 196 pp

Johan Z, Johan V (2005) Accessory minerals of the Cínovec (Zinnwald) granite cupola, Czech Republic: indicators of petrogenetic evolution. Mineral Petrol 83:113–150

Lisowiec K, Buzyn B, Slaby E, Renno AD, Götze J (2012) Fluid-induced magmatic and post-magmatic zircon and monazite patterns in granitoid pluton and related rhyolitic bodies. Chem Erde–Geochem 73(2):163–179

London D (2014) Subsolidus isothermal fractional crystallization. Am Mineral 99:543–546

Long KR, Van Gosen BS, Foley NK, Cordier D (2010) The principal rare earth elements deposits of the United States – a summary of domestic deposits and a global perspective. US Geol Surv scientific investigations report 2010–5220. US Geol Surv, Reston, 96 pp

Matthews WK III, Adams JAS (1986) Geochemistry, age, and structure of the Sierra Blanca and Finlay Mountain intrusions, Hudspeth County, Texas. Bureau of Economic Geology, University of Texas at Austin. Guidebook no 23, pp 207–224

McAnulty WN (1980) Geology and mineralization of the Sierra Blanca peaks, Hudspeth County, Texas. New Mexico Geol Soc, Socorro. Guidebook no 31, pp 263–266

Muehlberger WR (1980) Texas Lineament revisited. New Mexico Geol Soc, Socorro. Guidebook no 31, pp 113–121

Muller A, Seltman R, Kober B, Eklund O, Jeffries T, Kronz A (2008) Compositional zoning of rapakivi feldspars and coexisting quartz phenocrysts. Can Mineral 46:1417–1442

Muller A, van der Kerkhof AM, Behr HJ, Kronz A, Koch-Muller M (2009) The evolution of late-Hercynian granites and rhyolites documented by quartz – a review. Earth Env Sci ´T R So 100(1–2):185–204

Nesse WD (2000) Introduction to mineralogy. Oxford University Press, New York, 442 pp

O'Neill LC (2014) REE-Be-U-F mineralization of the Round Top laccolith, Sierra Blanca peaks, Trans-Pecos Texas. MSc thesis, University of Texas at Austin

Pingitore N, Clague J, Gorski D (2014) Round Top Mountain rhyolite (Texas, USA), a massive, unique Y bearing-fluorite-hosted heavy rare earth element (HREE) deposit. J Rare Earths 32(1):90–96

Price JG, Henry CD, Barker DS, Parker DF (1987) Alkalic rocks of contrasting tectonic settings in Trans-Pecos Texas. In: Mullen Morris E, Pasteris JD (eds) Mantle metasomatism and alkaline magmatism, Geol Soc Am Spec Pap, vol 215. Boulder, Geological Soc Am, pp 335–346

Price JG, Rubin JN, Henry CD, Pinkston TL, Tweedy SW, Koppenaal DW (1990) Rare-metal enriched peraluminous rhyolites in a continental arc, Sierra Blanca area, Trans-Pecos Texas; chemical modification by vapor-phase crystallization. In: Stein HJ, Hannah JL (eds) Ore-bearing granite systems; Petrogenesis and mineralizing processes, Geol Soc Am Spec Pap, vol 215. Boulder, Geological Soc Am, pp 335–346

Rubin JN, Price JG, Henry CD, Koppenaal DW (1987) Cryolite-bearing and rare metal-enriched rhyolite, Sierra Blanca peaks, Hudspeth County, Texas. Am Mineral 72(11–12):1122–1130

Rubin JN, Henry CD, Price JG (1989a) Hydrothermal zircons and zircon overgrowths, Sierra Blanca peaks. Texas: Am Mineral 74(7–8):865–869

Rubin JN, Price JG, Henry CD, Pinkston TL, Tweedy SW, Koppenaal DW, Peterson SB, Harlan HM, Miller WT, Thompson RJ, Grabowski RB, Laybourn PD, Schrock GE, Johnson A, Staes DG, Gaines RV, Miller FH (1989b) Mineralogy of beryllium deposits near Sierra Blanca, Texas. Proc Metal 5:601–614

Rubin JN, Price JG, Henry CD, Kyle JR (1990) Geology of the beryllium-rare earth element deposits at Sierra Blanca, West Texas. In: Kyle JR (ed) Industrial mineral ressources of the Delaware Basin, Texas and New Mexico. Guidebook series, vol 8. Littleton, Soc Econ Geol, pp 191–203

Rubin JN, Henry CD, Pinkston TL, Tweedy SW, Koppenaal DW (1993) The mobility of zirconium and other 'immobile' elements during hydrothermal alteration. Chem Geol 110(1–3):29–47

Shannon WM (1986) Lithogeochemical characterization of intrusive rocks comprising the Quitman-Sierra Blanca igneous complex, Hudspeth County, Texas. MSc thesis, University of Texas at El Paso

Shannon WM, Goodell PC (1986) Lithogeochemistry of intrusive rocks of the Quitman-Sierra Blanca igneous complex, Hudspeth County, Texas. Bureau of Economic Geology, University of Texas at Austin, Guidebook no 23, pp 225–236

Shelley D (1992) Igneous and metamorphic rocks under the microscope: classification, textures, microstructures and mineral preferred-orientations. Chapman & Hall London, 450 pp

Vernon RH (2004) A practical guide to rock microstructure. Cambridge University Press, Cambridge, 606 pp

Wilson JA (1980) Geochronology of the Trans-Pecos Texas volcanic field. New Mexico Geol Soc, Socorro. Guidebook no 31:205–211

Zachariansen WH (1951) Crystal chemical studies of the 5f-series of elements. XIV. Oxyfluorides, XOF. Acta Crystallogr 4:231–236